A tool to obtain the coefficients of thermal expansion for CFRP composites using full-field data fusion

Rafael Ruiz Iglesias

R. Cappello, G. Ólafsson, O.T. Thomsen and J.M. Dulieu-Barton

PhD Student

THERMOELASTIC STRESS ANALYSIS (TSA)

T_0 ~ *Mean temperature*
ρ ~ *Density*
C_p ~ *Specific heat capacity*
α_1 *and* α_2 ~ *Thermal expansion coefficients in 1,2*
$\Delta\sigma_1$ *and* $\Delta\sigma_2$ ~ *Stress variation in 1,2*
$[Q]_{1,2}$ ~ *Stiffness matrix*
$[T]$ ~ *Transformation matrix*
$[\Delta\varepsilon_{xy}]$ ~ *Strain variation in x,y*

Stress variation (Δσ) is required to obtain the **thermoelastic response** of a material:

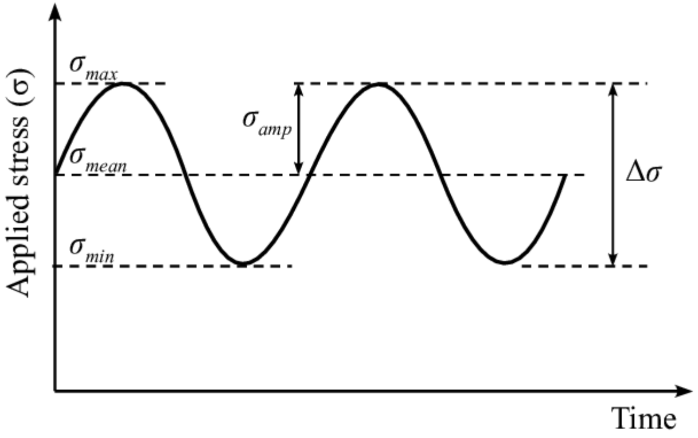

$$\Delta T = \frac{-T_0}{\rho C_p}(\alpha_1\Delta\sigma_1+\alpha_2\Delta\sigma_2) = \frac{-T_0}{\rho C_p}\left([\alpha]_{1,2}^{T}[Q]_{1,2}[T][\Delta\varepsilon]_{xy}\right)$$

Simplified for orthotropic composite lamina (as $\alpha_6 = 0$)

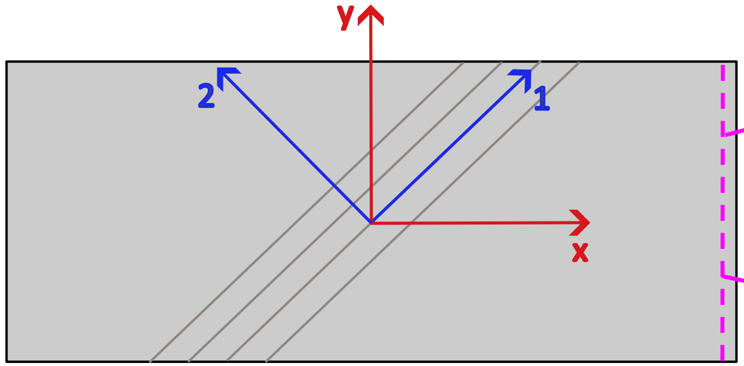

1,2: Ply coordinate system

x,y: Laminate coordinate system

Cross- section

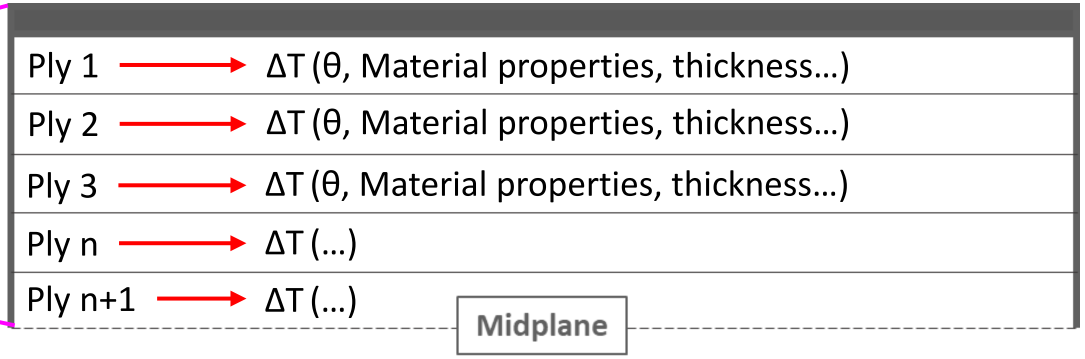

Cross-section of multi-directional symmetric laminate

Full Field Imaging of MD CFRP

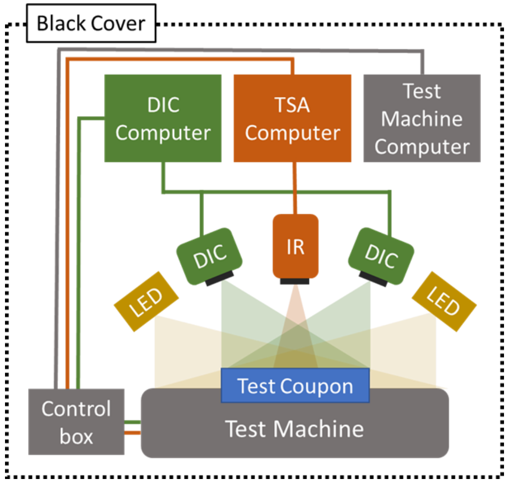

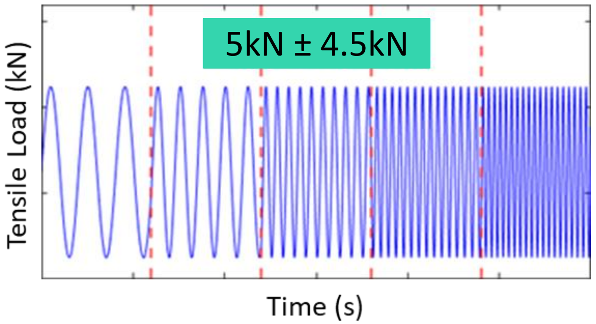

Cyclic test **below FPF**

Loading frequency (Hz): 0.5, 1.1, 2.1, 3.1, 4.1, 5.1, 7.1, 10.1... 30.1

CFRP IM7/8552: Heat transfer occurring at low frequencies [1]

Widely used in the aerospace industry

Multidirectional Specimen Strips Preparation

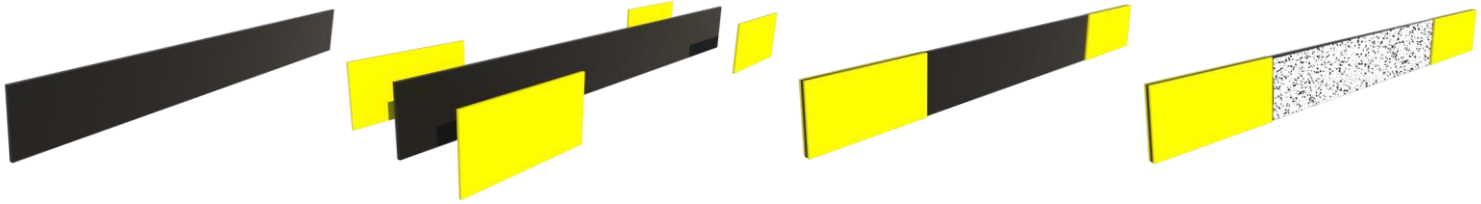

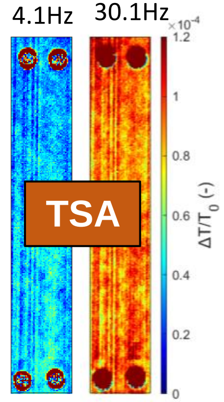

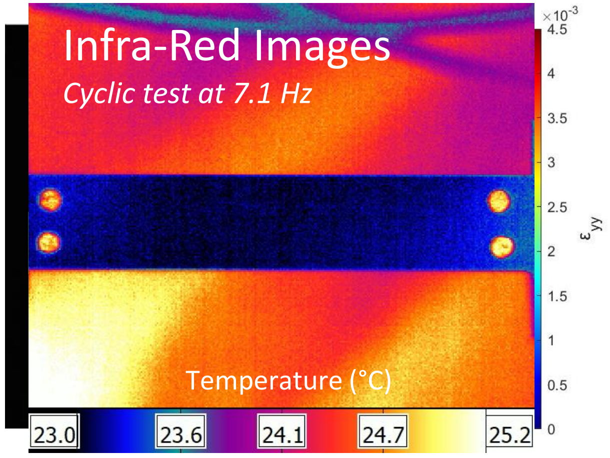

[1] Jiménez-Fortunato I., Bull DJ., Thomsen OT., Dulieu-Barton JM. On the source of the thermoelastic response from orthotropic fibre reinforced composite laminates. Composites Part A: Applied Science and Manufacturing

Thermoelastic Response of the MD CFRP laminates

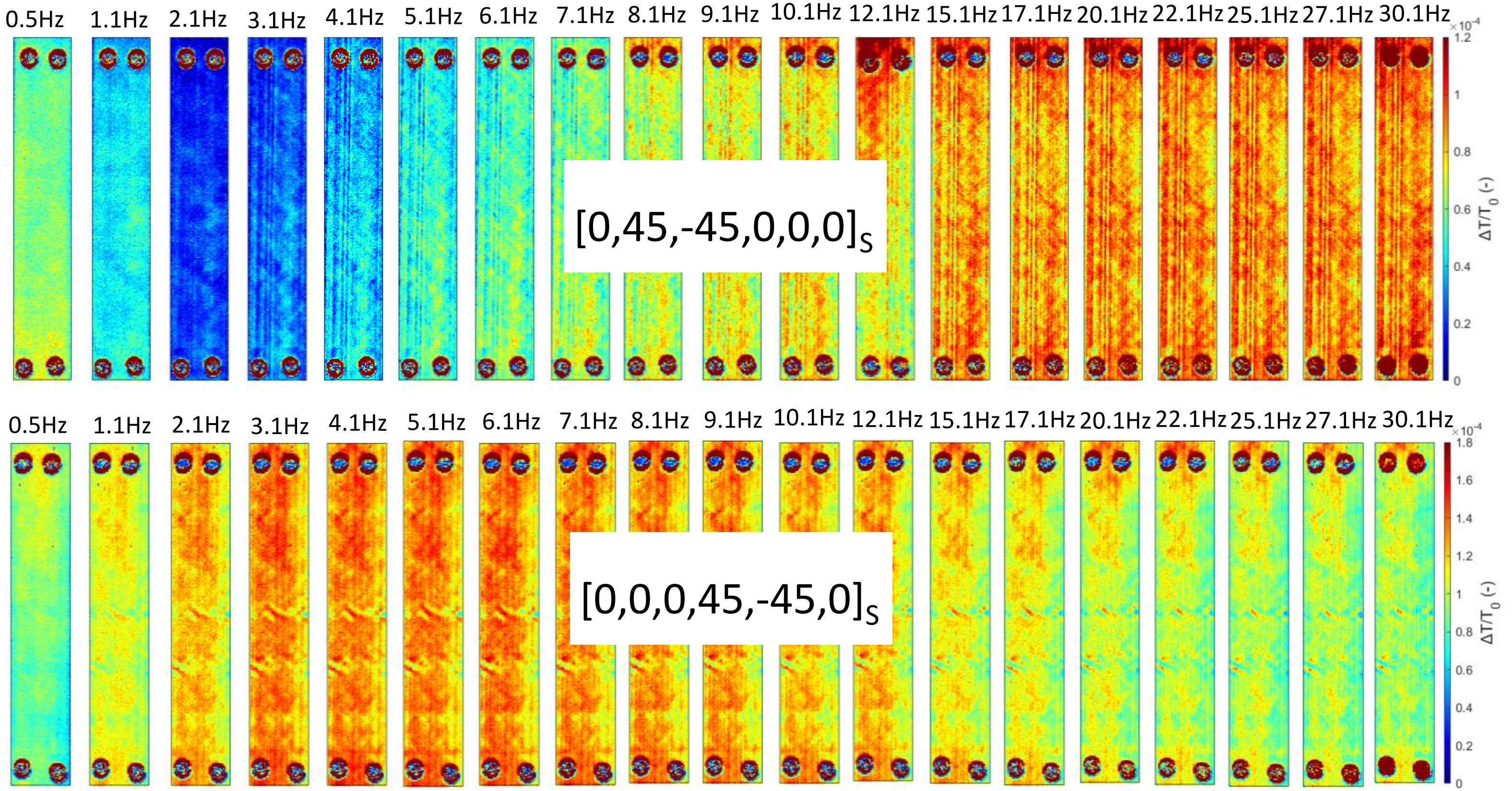

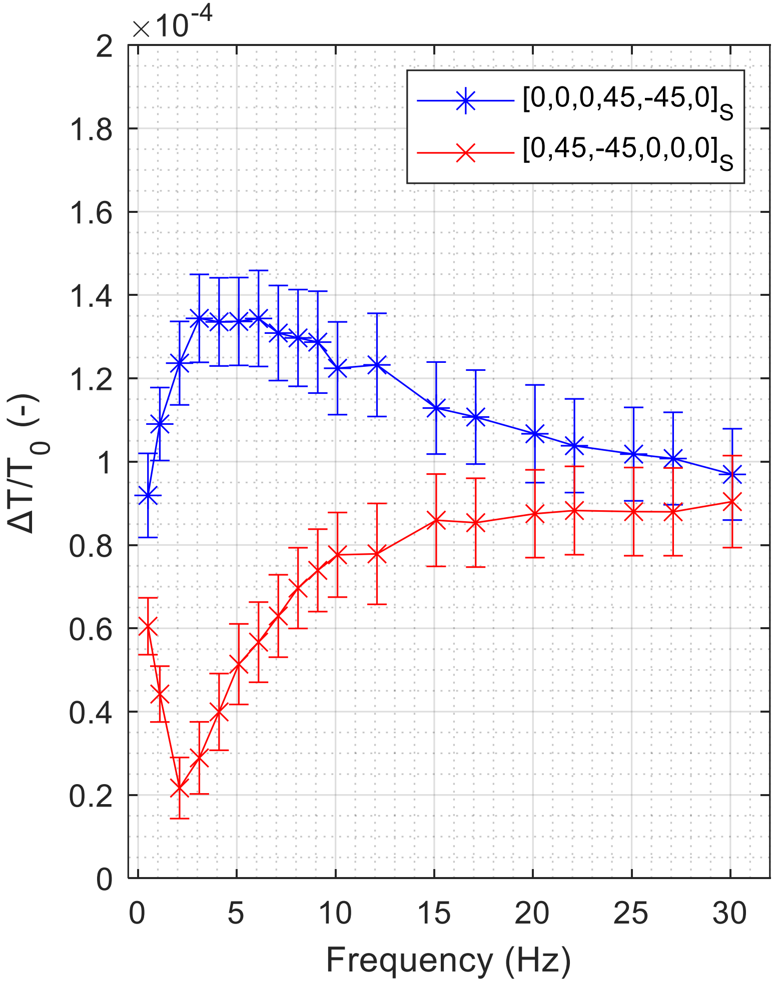

Full field ***$\Delta T/T_0$*** show a **homogeneous** distribution through the laminate surface

The **stress/strain** state throughout the surface **is homogeneous too**

No constant HEAT TRANSFER uency range

ΔT is different from 0 to 45-degree plies

FULL FIELD DATA PROCESSING & FUSION

TSA Raw Data

output: Images

Lock-In Algorithm

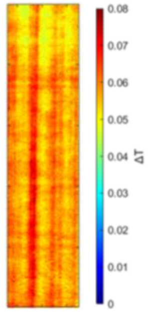

Final output: *ΔT, T_0, phase*

Compare

Thermomechanical models

Wong's model

- Numerical model
- 1D model
- Orientation, L.F, resin surface layer…
- Material properties

Final output: ΔT_{Models}

DIC Raw Data

output: Images

MatchID Software

output: *Displacement*

output: Strains

Lock-in Algorithm

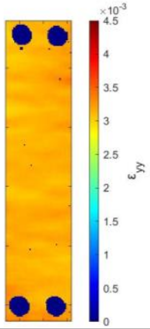

Final output: *$\Delta Strain$*

INPUT

**Homogeneous in the laminate surface*

MOTIVATION OF THE RESEARCH

List of CFRP IM7/8552 mechanical and thermal properties from multiple references (will be shown at the end of the presentation)

Reference	[1]	[2]	[3]	[4]	[5]	[6]	[7]	[8]	% Variation
Young's modulus E_1 (GPa)	148.8	171.4	161.0	164.0	161.0	158.5	161.0	165.0	22.26
Young's modulus E_2 (GPa)	9.19	9.08	11.38	12.00	11.38	8.96	11.38	9.00	15.29
Poisson's ratio ν_{12}	0.34	0.32	0.32	0.30	0.32	0.32	0.32	0.34	0.04
Bending stiffness G_{12} (GPa)	5.06	5.30	5.17	5.00	5.20	4.69	5.17	5.60	1.14
Thermal expansion coeff. α_1 (10^{-6} K^{-1})	-0.3	-5.5	-0.1	-0.1	-0.9	-0.17	0	-1.0	298.12
Thermal expansion coeff. α_2 (10^{-6} K^{-1})	28.4	25.5	31	12.4	28.8	36.5	30	18	196.20

$$\alpha(T) = \frac{1}{l(T)} \frac{dl}{dT}$$

- Residual stress
- Undesired deformation

Residual stress induced cracks

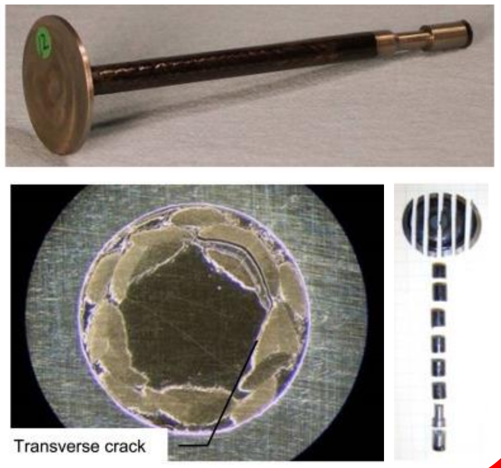

Manufacturing induced deformation

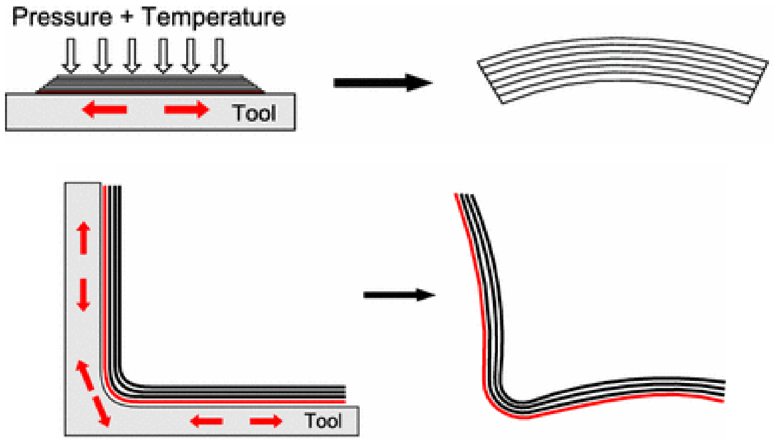

Dimensional stability

MOTIVATION OF THE RESEARCH

List of CFRP IM7/8552 mechanical and thermal properties from multiple references (will be shown at the end of the presentation)

Reference	[1]	[2]	[3]	[4]	[5]	[6]	[7]	[8]	% Variation
Young's modulus E_1 (GPa)	148.8	171.4	161.0	164.0	161.0	158.5	161.0	165.0	22.26
Young's modulus E_2 (GPa)	9.19	9.08	11.38	12.00	11.38	8.96	11.38	9.00	15.29
Poisson's ratio ν_{12}	0.34	0.32	0.32	0.30	0.32	0.32	0.32	0.34	0.04
Bending stiffness G_{12} (GPa)	5.06	5.30	5.17	5.00	5.20	4.69	5.17	5.60	1.14
Thermal expansion coeff. α_1 (10^{-6} K^{-1})	-0.3	-5.5	-0.1	-0.1	-0.9	-0.17	0	-1.0	298.12
Thermal expansion coeff. α_2 (10^{-6} K^{-1})	28.4	25.5	31	12.4	28.8	36.5	30	18	196.20

$$\alpha(T) = \frac{1}{l(T)}\frac{dl}{dT}$$

- Residual stress
- Undesired deformation

Residual stress induced cracks

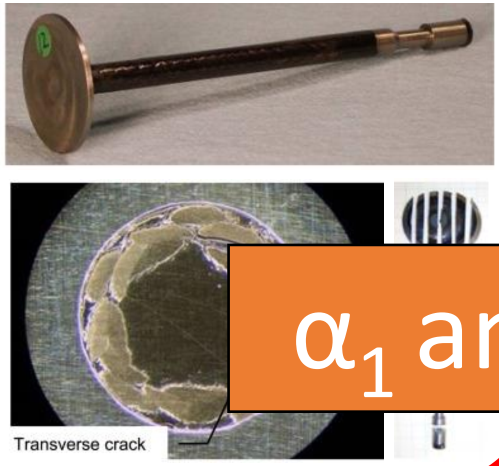

Manufacturing induced deformation

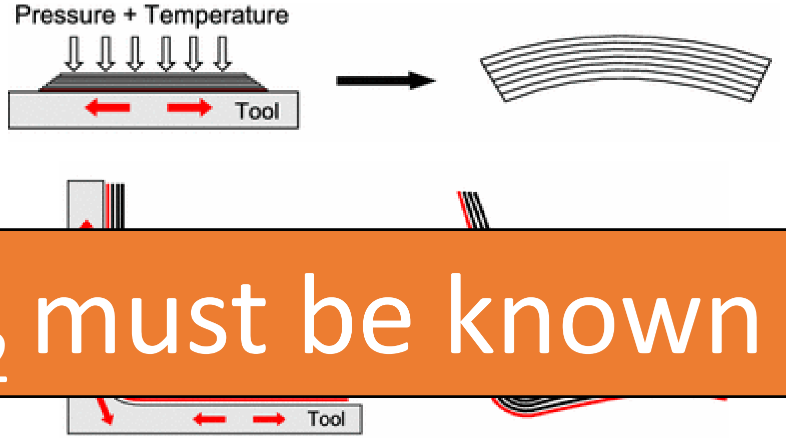

Dimensional stability

α_1 and α_2 must be known values!

MOTIVATION OF THE RESEARCH

List of CFRP IM7/8552 mechanical and thermal properties from multiple references (will be shown at the end of the presentation)

Reference	[1]	[2]	[3]	[4]	[5]	[6]	[7]	[8]	% Variation
Young's modulus E_1 (GPa)	148.8	171.4	161.0	164.0	161.0	158.5	161.0	165.0	22.26
Young's modulus E_2 (GPa)	9.19	9.08	11.38	12.00	11.38	8.96	11.38	9.00	15.29
Poisson's ratio ν_{12}	0.34	0.32	0.32	0.30	0.32	0.32	0.32	0.34	0.04
Bending stiffness G_{12} (GPa)	5.06	5.30	5.17	5.00	5.20	4.69	5.17	5.60	1.14
Thermal expansion coeff. α_1 (10^{-6} K^{-1})	-0.3	-5.5	-0.1	-0.1	-0.9	-0.17	0	-1.0	298.12
Thermal expansion coeff. α_2 (10^{-6} K^{-1})	28.4	25.5	31	12.4	28.8	36.5	30	18	196.20

$$\alpha(T) = \frac{1}{l(T)}\frac{dl}{dT}$$

- Residual stress
- Undesired deformation

AIM & OBJECTIVES → **Device a quick and reliable tool for obtaining the CTEs from CFRP**

- Use simple strip **multidirectional specimens** loaded in uniaxial cyclic tension at different loading frequencies.
- Use **Thermoelastic Stress Analysis (TSA) and Digital Image Correlation (DIC)** to obtain $\Delta T/T_0$ and the strains
- Use an **optimization procedure** based on a **comparison of an analytical model of heat transfer** with the experimental data to **identify the CTEs**

α_1 and α_2 must be known values!

$\Delta T/T_0$ from Wong's model using values in [1-8]

Wong's model is used inputting IM7/8552 properties mentioned in Table 1.

$[0,45,-45,0,0,0]_S$

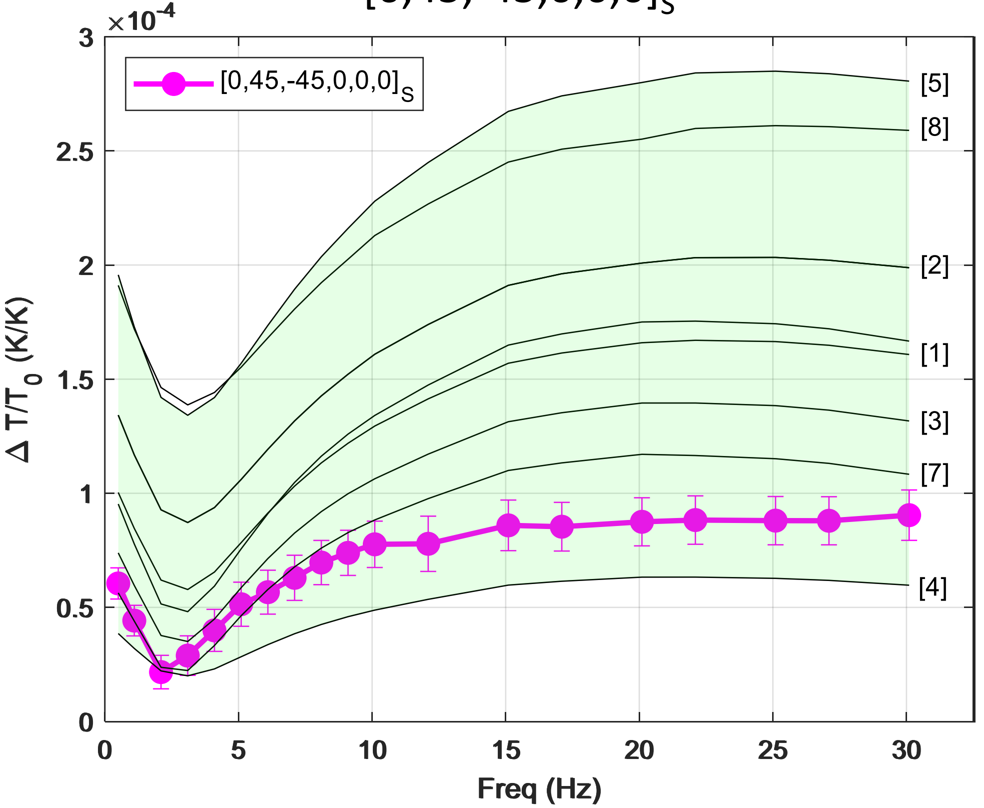

$[0,0,0,45,-45,0]_S$

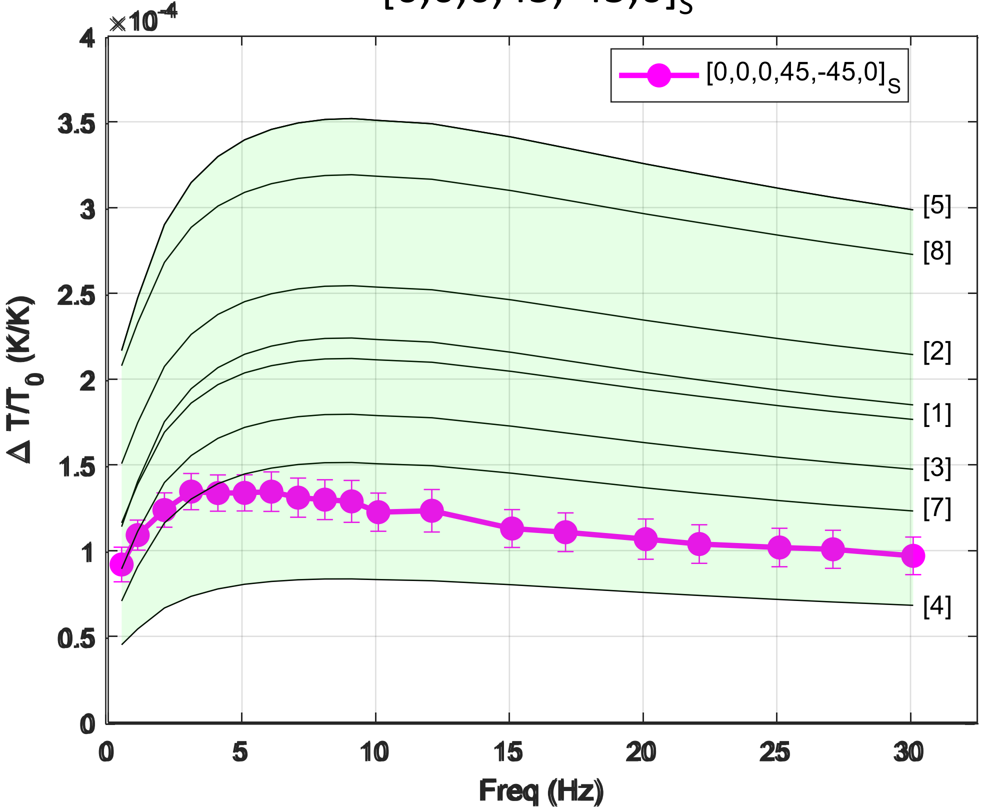

Trend in the respons   Let's put the experimental results here   which is correct?

CTE IDENTIFICATION METHODOLOGY

Lock-In Algorithm

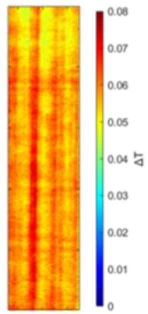

Final output: ***ΔT, T_0, phase***

Least Squares Algorithm

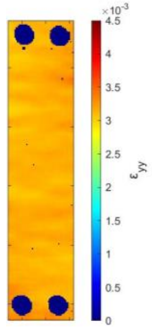

Final output: ***ΔStrain***

Optimization Process

Find local minima of a target function

It is very important to clearly define the **α_1 and α_2 range**

Target function

$$F(\alpha_1,\alpha_2) = \left(\frac{\Delta T}{T_0}\right)_{TSA} - \left(\frac{\Delta T}{T_0}(\alpha_1,\alpha_2)\right)_{Wongs\ Model}$$

Wong's model [10]

- Material properties are needed (E_1,E_2,G_{12}, ν_{12})
- Resin Rich Layer (RRL) must be measured
- Resin properties are required (E_r ,G_r ,ν_r)
- Strains are needed ✔

Unkonws: α_1 and α_2

A **physical plausible range** must be defined!

Result

α_1 and α_2

Min ($\Delta T/T_{0\,TSA} - \Delta T/T_{0\,model}$)

IM7/8552 MATERIAL PROPERTIES OBTENTION

Constituents' properties of the fibre and the resin

IM7 Fibre Reference	[11]	[12]	[13]	[14]	[15]	[16]	[17]	[18]	CV (%)
Young's modulus E_{1f} (GPa)	276	X	X	276	X	276	276	263.7	2.01
Young's modulus E_{2f} (GPa)	X	X	X	56	X	19.5	15	19	70.10
Poisson's ratio ν_f	0.22	X	X	0.32	X	0.28	0.2	0.2	21.99
Bending stiffness G_f (GPa)	X	X	X	28	X	70	15	27.6	68.29
Density ρ_f (kg m^{-3})	1780	X	X	X	X	1780	1780	X	0.00
Specific heat capacity Cp_f (J kg^{-1} K^{-1})	879.2	X	X	X	X	879	X	X	0.02
Thermal expansion coeff. α_{1f} (10^{-6} K^{-1})	-0.64	-0.4	-0.9	-2.29	-1	-0.54	X	-0.4	75.21
Thermal expansion coeff. α_{2f} (10^{-6} K^{-1})	X	4.4 ~ 6.6	7.2	9.2	10	10.08	X	5.63	30.86

8552 Resin Reference	[1]	[4]	[7]	[8]	[19]	[20]	CV (%)
Young's modulus E_{1r} (GPa)	3.8	5	4.67	4.08	X	X	12.45
Poisson's ratio ν_r	0.35	0.40	0.33	0.38	X	X	8.52
Bending stiffness G_r (GPa)	1.41	X	X	1.48	X	X	3.43
Density ρ_r (kg m^{-3})	1153	X	X	X	1301	1300	6.81
Specific heat capacity Cp_r (J kg^{-1} K^{-1})	1100	X	X	X	1350	1025	14.69
Thermal expansion coeff. α_r (10^{-6} K^{-1})	53.5	60	65	46.7	48.0	X	14.31

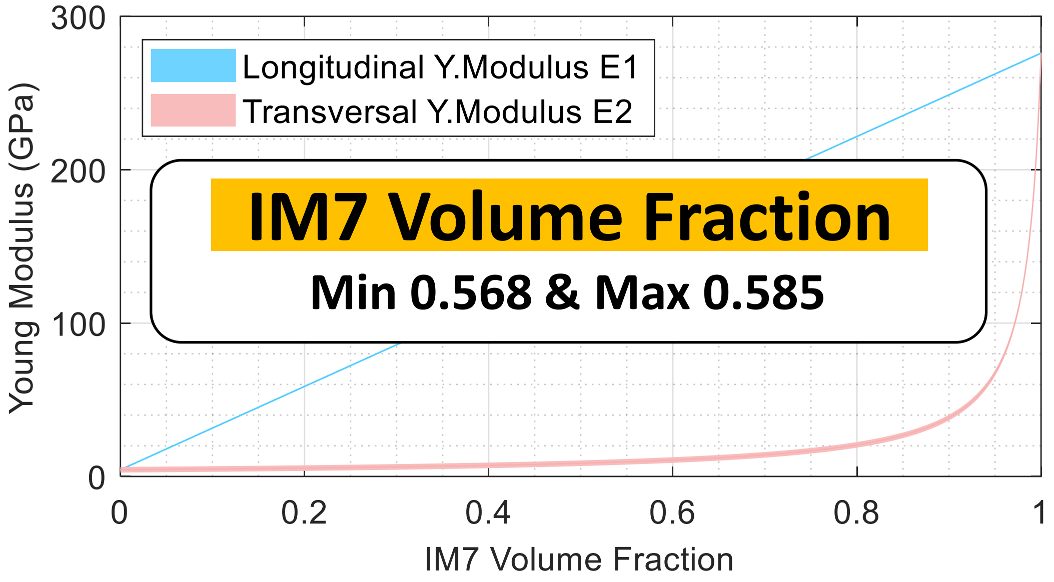

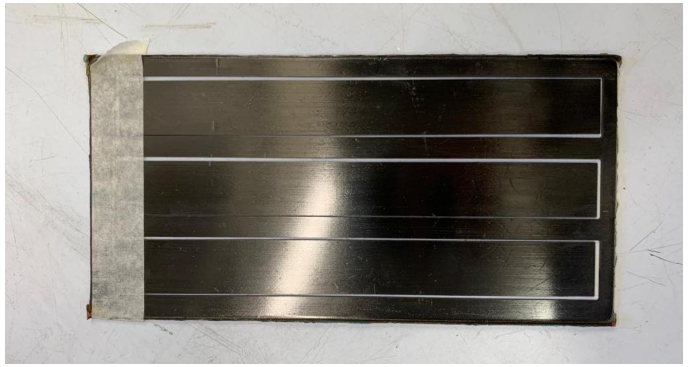

$[0]_{18}$ CFRP $[90]_{18}$ CFRP

Tension tests were first performed **on x3 CFRP $[0]_{18}$ and $[90]_{18}$**

Experimental results

E_1 Mean
E_1 STD

&

E_2 Mean
E_2 STD

IM7/8552 MATERIAL PROPERTIES OBTENTION

Constituents' properties of the fibre and the resin

IM7 Fibre Reference	[11]	[12]	[13]	[14]	[15]	[16]	[17]	[18]	CV (%)
Young's modulus E_{1f} (GPa)	276	X	X	276	X	276	276	263.7	2.01
Young's modulus E_{2f} (GPa)	X	X	X	56	X	19.5	15	19	70.10
Poisson's ratio ν_f	0.22	X	X	0.32	X	0.28	0.2	0.2	21.99
Bending stiffness G_f (GPa)	X	X	X	28	X	70	15	27.6	68.29
Density ρ_f (kg m^{-3})	1780	X	X	X	X	1780	1780	X	0.00
Specific heat capacity Cp_f (J kg^{-1} K^{-1})	879.2	X	X	X	X	879	X	X	0.02
Thermal expansion coeff. α_{1f} (10^{-6} K^{-1})	-0.64	-0.4	-0.9	-2.29	-1	-0.54	X	-0.4	75.21
Thermal expansion coeff. α_{2f} (10^{-6} K^{-1})	X	4.4 ~ 6.6	7.2	9.2	10	10.08	X	5.63	30.86

8552 Resin Reference	[1]	[4]	[7]	[8]	[19]	[20]	CV (%)
Young's modulus E_{1r} (GPa)	3.8	5	4.67	4.08	X	X	12.45
Poisson's ratio ν_r	0.35	0.40	0.33	0.38	X	X	8.52
Bending stiffness G_r (GPa)	1.41	X	X	1.48	X	X	3.43
Density ρ_r (kg m^{-3})	1153	X	X	X	1301	1300	6.81
Specific heat capacity Cp_r (J kg^{-1} K^{-1})	1100	X	X	X	1350	1025	14.69
Thermal expansion coeff. α_r (10^{-6} K^{-1})	53.5	60	65	46.7	48.0	X	14.31

Tension tests were first performed **on x3 CFRP $[0]_{18}$ and $[90]_{18}$**

Experimental results

E_1 Mean
E_1 STD

&

E_2 Mean
E_2 STD

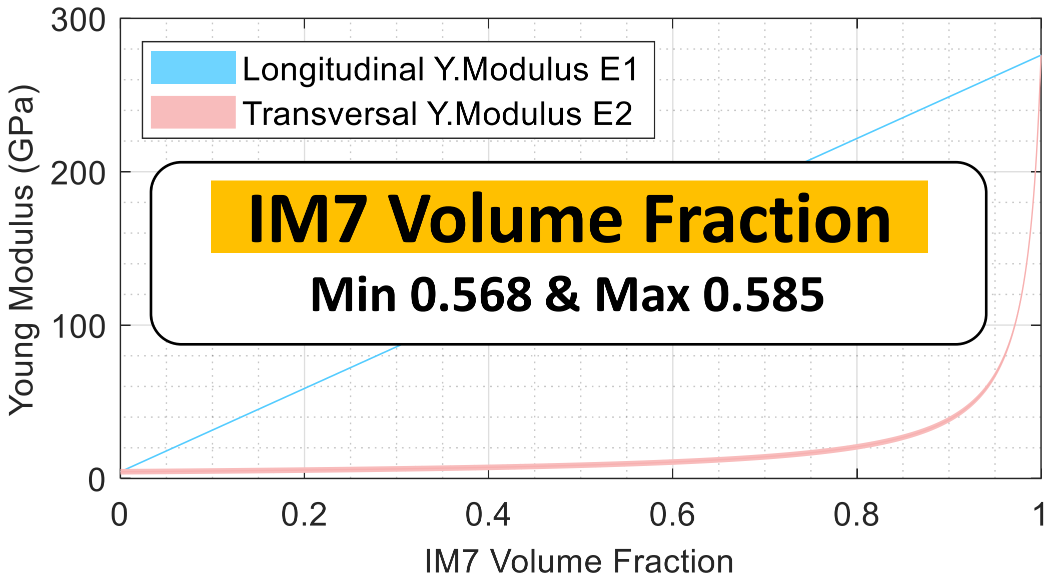

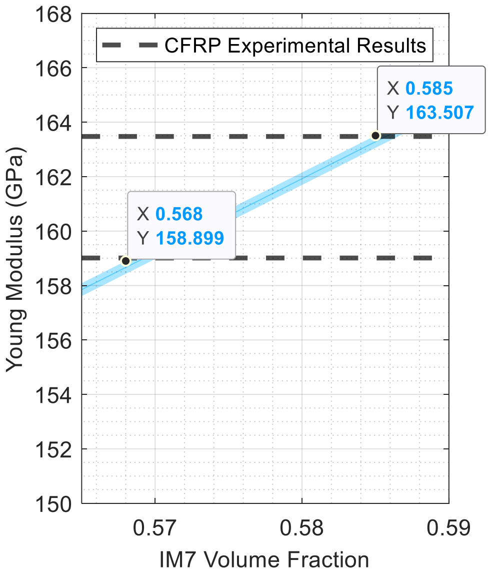

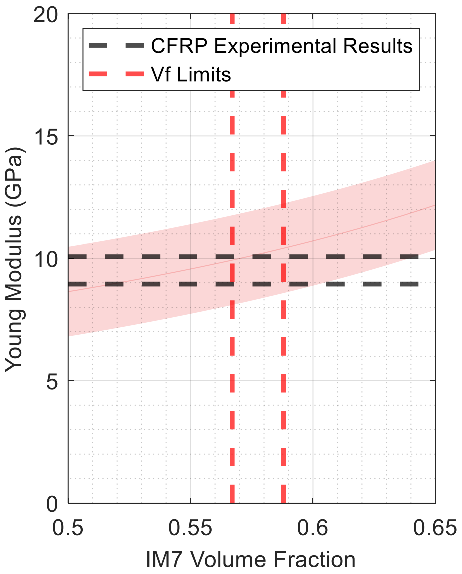

RELIABLE BOUNDS FOR THE CTE OBTENTION

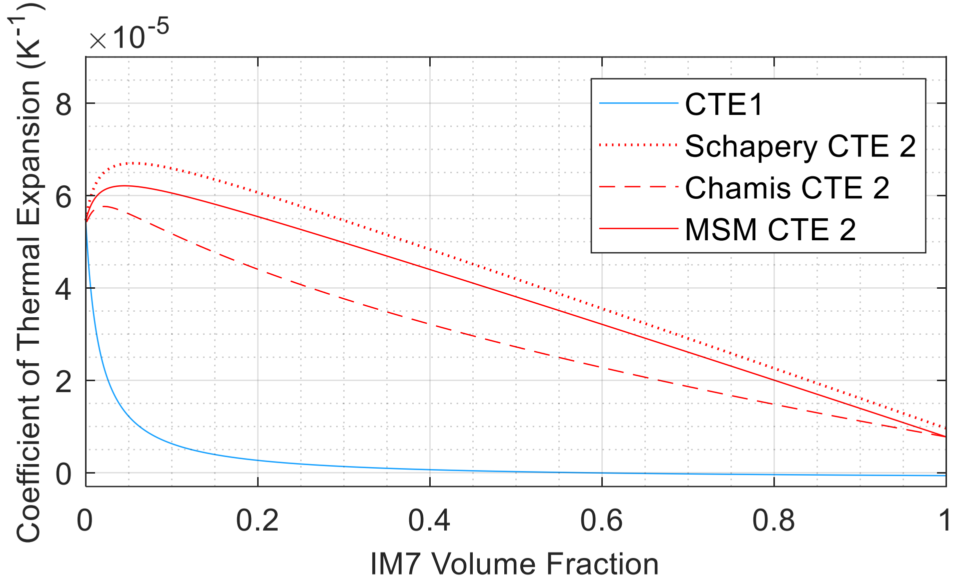

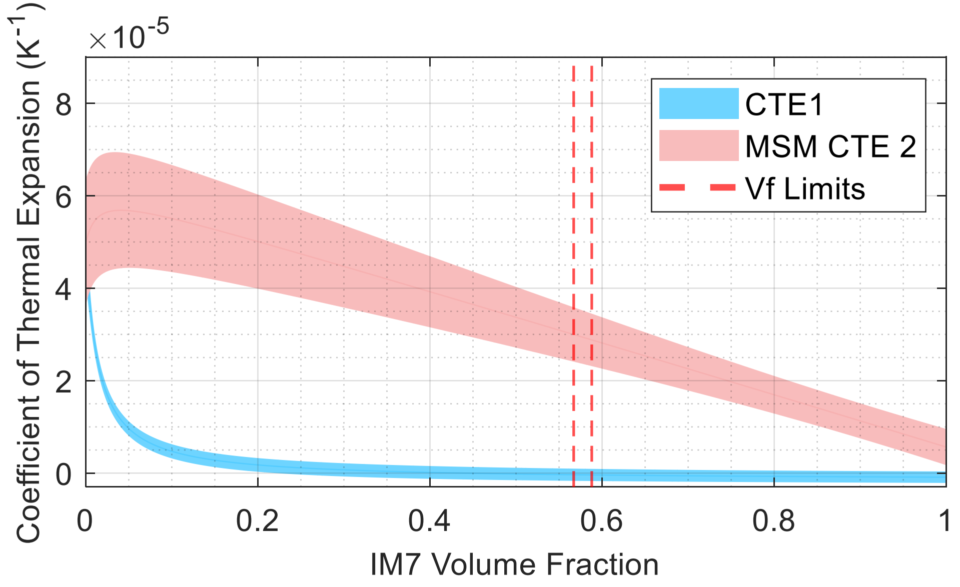

- α_1 swaps in sign around 0.5 IM7 Volume fraction
- Hashin and the **MSM** models give the best fit for α_2 [21]

Constituents' properties of the fibre and the resin

IM7 Fibre Reference	[11]	[12]	[13]	[14]	[15]	[16]	[17]	[18]	CV (%)
Thermal expansion coeff. α_{1f} (10^{-6} K^{-1})	-0.64	-0.4	-0.9	-2.29	-1	-0.54	X	-0.4	75.21
Thermal expansion coeff. α_{2f} (10^{-6} K^{-1})	X	4.4 ~ 6.6	7.2	9.2	10	10.08	X	5.63	30.86

8552 Resin Reference	[1]	[4]	[7]	[8]	[19]	[20]	CV (%)
Thermal expansion coeff. α_r (10^{-6} K^{-1})	53.5	60	65	46.7	48.0	X	14.31

Range of possible CTEs from micromechanical models.

Material property	Lower limit	Upper limit
Thermal expansion coeff. α_1 (10^{-6} K^{-1})	-1.610	$\boxed{0.974}$
Thermal expansion coeff. α_2 (10^{-6} K^{-1})	22.131	35.864

Physical plausible limits for CTEs

TSA Results from the UD specimens

Tension cyclic tests were also performed **on x3 CFRP $[0]_{18}$ and $[90]_{18}$**

CFRP $[90]_{18}$ → 0.3kN ± 0.2kN

CFRP $[0]_{18}$ → 3kN ± 2kN

L. Frequency: 1.1,10.1 and 20.1 Hz

- No damage is induced
- Different thermoelastic response
- **Phase (θ)**

Physical plausible limits for CTEs

Material property	Lower limit	Upper limit
CTE α_1 (10^{-6} K^{-1})	-1.610	$\boxed{0.974}$
CTE α_2 (10^{-6} K^{-1})	22.131	35.864

IM7/8552 α_1 must be

Negative

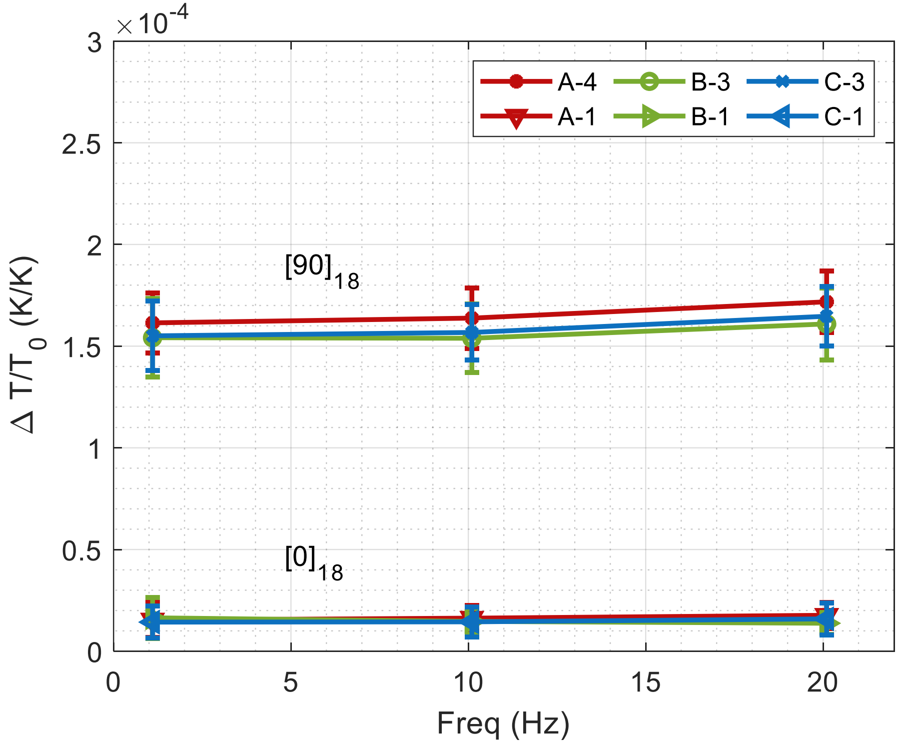

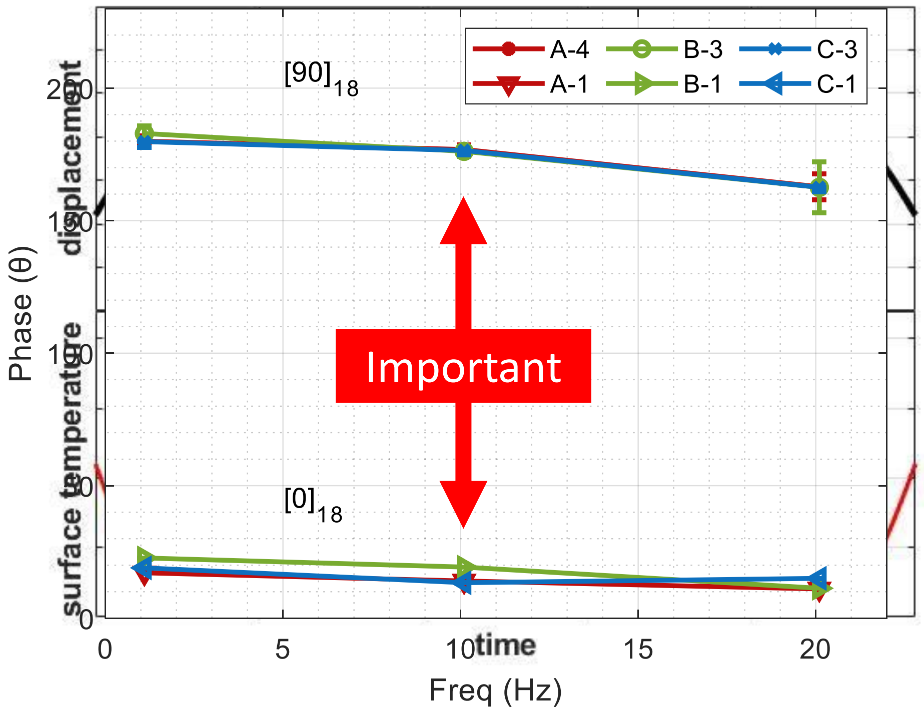

CFRP OPTIMISED CTEs and TSA response

The optimization process was done for all frequencies of $[0,45,-45,0,0,0]_S$ & $[0,0,0,45,-45,0]_S$

Mean and std for α_1 & α_2

**Must be similar for both configurations*

Configuration	CTE α_1 (10^{-6} K^{-1})	CTE α_2 (10^{-6} K^{-1})
$[0,45,-45,0,0,0]_S$	-0.103083 ± 0.016737	24.125912 ± 3.608031
$[0,0,0,45,-45,0]_S$	-0.102046 ± 0.014819	22.151729 ± 3.217313
AVERAGE	-0.102564 ± 0.031618	23.138820 ± 6.821089

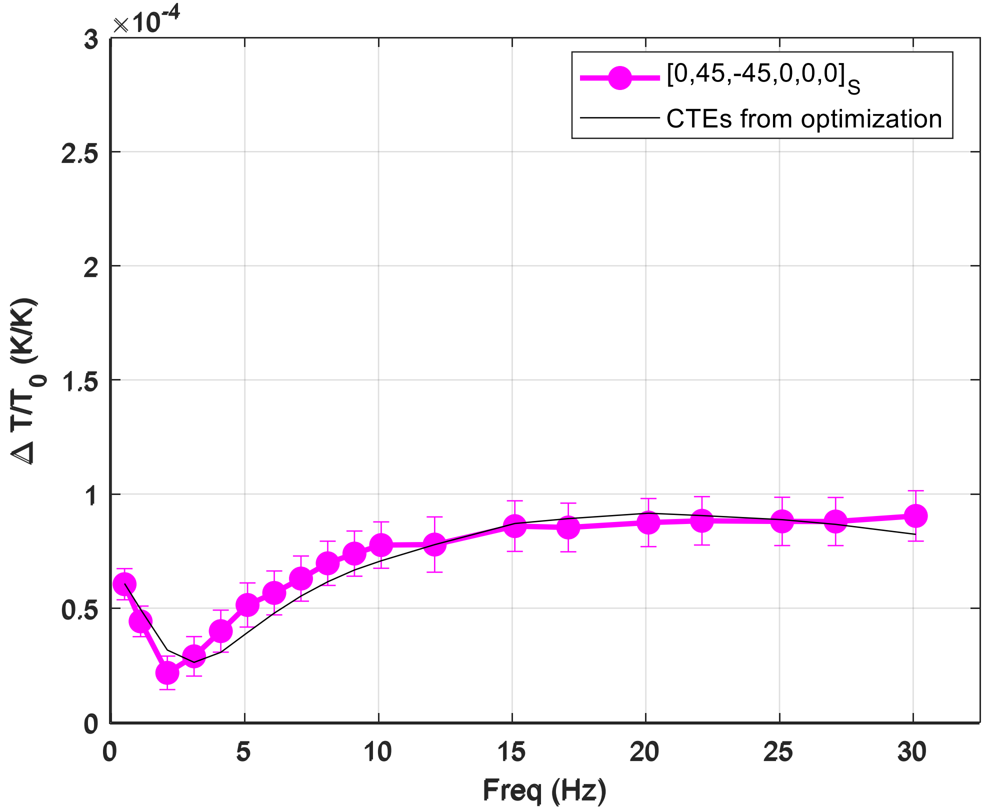

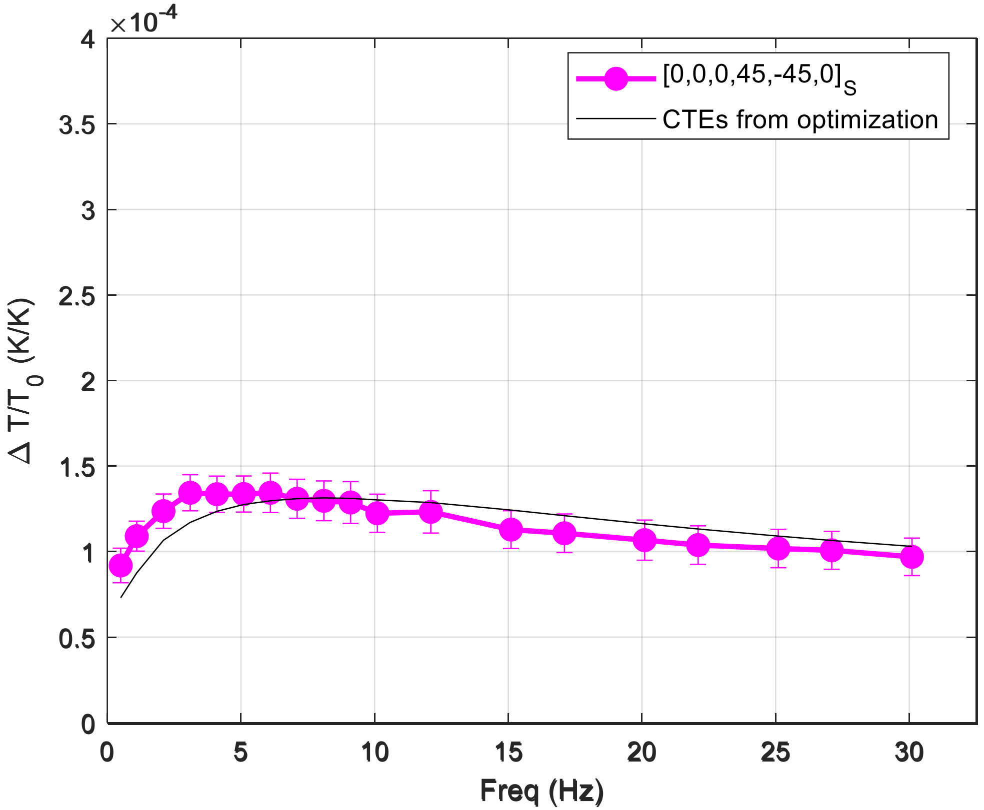

FFDF for detecting resin pockets in MD laminates

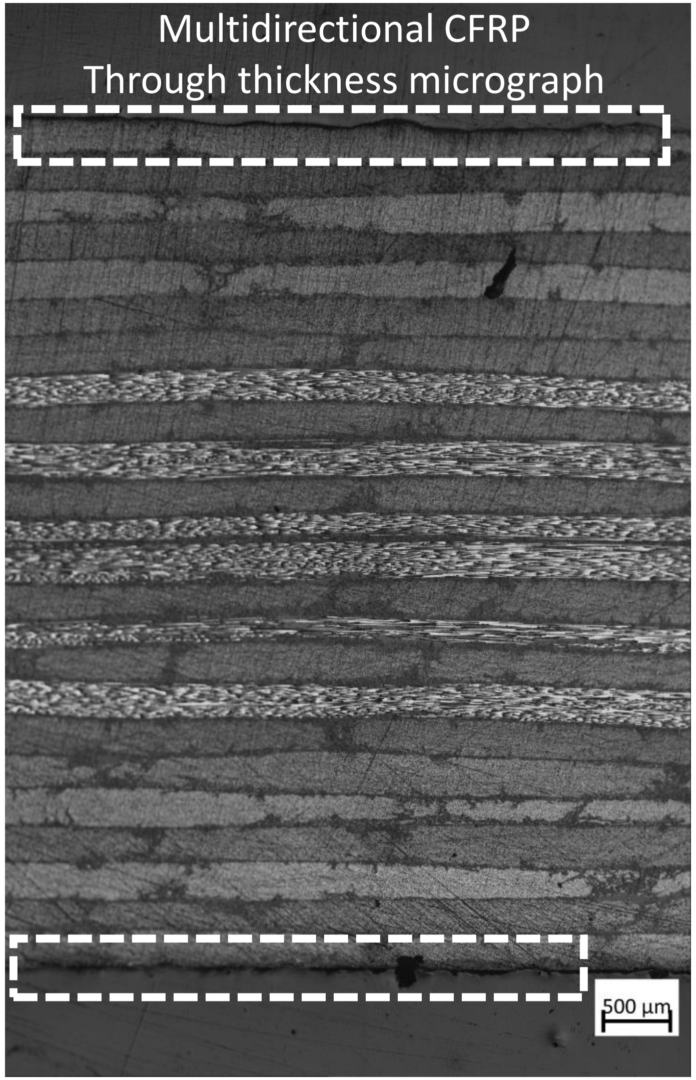

FFDF for detecting resin pockets in MD laminates

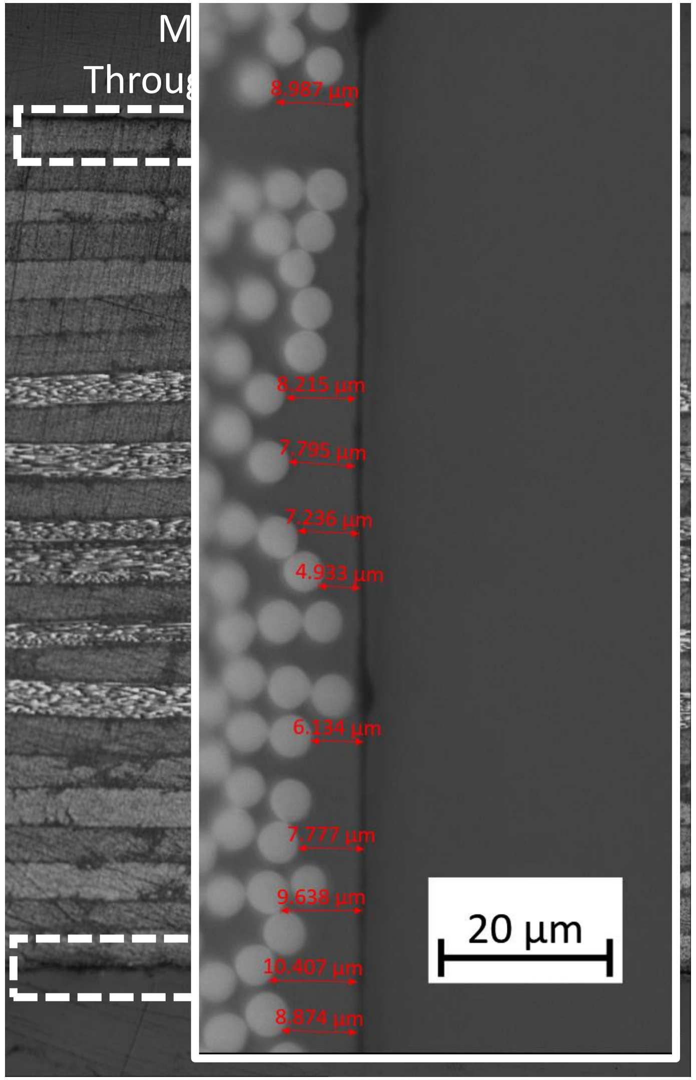

FFDF for detecting resin pockets in MD laminates

The thickness of the **RRL is not constant** through the entire imaged surface **and hence influences the response locally**.

Full field $\Delta T/T_0$ maps generated at 15.1Hz clearly show heterogeneities

α_1 is highly sensitive to variations in fibre/matrix volume fractions

positive or negative values when doing the full field analysis.

α_1 $(K^{-1}) \in [-0.3 \cdot 10^{-6}, 0.09 \cdot 10^{-6}]$

CFRP $[0,45,-45,0,0,0]_S$

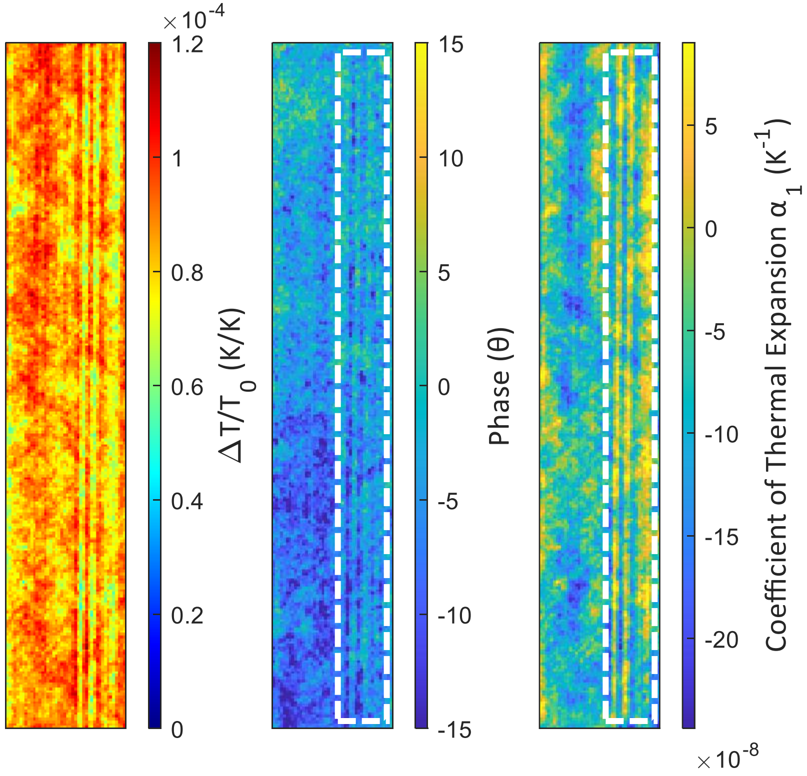

CFRP $[0,0,0,45,-45,0]_S$

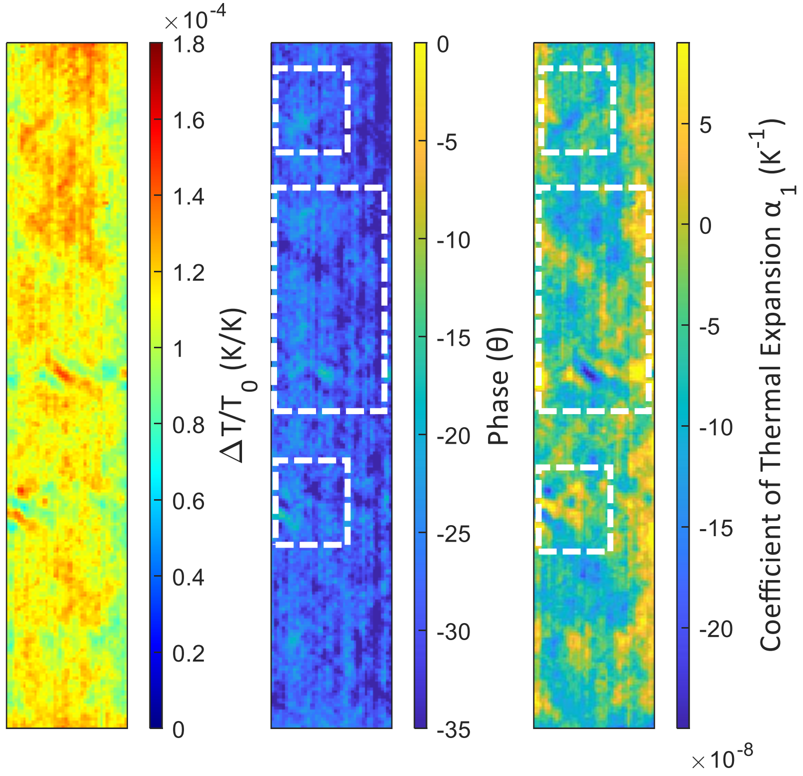

CONCLUSIONS

Feasible physical limits were first established **for the laminae properties**

- α_1 (K^{-1}) $\in [-0.161 \cdot 10^{-6}, 0]$ and α_2 (K^{-1}) $\in [22.131 \cdot 10^{-6}, 35.864 \cdot 10^{-6}]$.

Possibility of **calculating α_1 and α_2 accurately** using an optimization algorithm as the $\Delta T/T_0$ is very sensible to the CTEs

1. The multidirectional laminates $\alpha_1 \approx -0.103 \cdot 10^{-6}\ K^{-1}$ and $\alpha_2 \approx 23.139 \cdot 10^{-6}\ K^{-1}$

Resin pockets in the surface **have been identified** combining the TSA Phase and variations in α_1

FUTURE WORK

- **Confirm results** found with another experimental technique (e.g. resin concentration with X-Ray CT Scanning)
- Real structure?: **C-Spar** (If there is enough time)
- Different stress states (e.g. bending)

REFERENCES

1. Jiménez-Fortunato I., Bull DJ., Thomsen OT., Dulieu-Barton JM. On the source of the thermoelastic response from orthotropic fibre reinforced composite laminates. Composites Part A: Applied Science and Manufacturing. Elsevier Ltd; 1 October 2021; 149(106515): 1–15.

2. Camanho PP., Maimí P., Dávila CG. Prediction of size effects in notched laminates using continuum damage mechanics. Composites Science and Technology. October 2007; 67(13): 2715–2727. Available at: DOI:10.1016/j.compscitech.2007.02.005

3. Stacey JP., O'Donnell MP., Schenk M. Thermal Prestress in Composite Compliant Shell Mechanisms. Volume 5A: 42nd Mechanisms and Robotics Conference. American Society of Mechanical Engineers; 2018. Available at: DOI:10.1115/DETC2018-85826

4. Daynes S., Potter KD., Weaver PM. Bistable prestressed buckled laminates. Composites Science and Technology. December 2008; 68(15–16): 3431–3437. Available at: DOI:10.1016/j.compscitech.2008.09.036

5. Krueger R. Finite Element Analysis of Composite Joint Configurations with Gaps and Overlaps. 2014. Available at: https://api.semanticscholar.org/CorpusID:134394354

6. Catinaccio A., Esala J. HTS Magnet CFRP Casing Conceptual Study. 2021.

7. Zhang B., Kawashita LF., Jones MI., Lander JK., Hallett SR. An experimental and numerical investigation into damage mechanisms in tapered laminates under tensile loading. Composites Part A: Applied Science and Manufacturing. June 2020; 133: 105862. Available at: DOI:10.1016/j.compositesa.2020.105862

8. Kaddour A., Hinton M., Smith P., Li S. Mechanical properties and details of composite laminates for the test cases used in the third world-wide failure exercise. Journal of Composite Materials. 19 September 2013; 47(20–21): 2427–2442. Available at: DOI:10.1177/0021998313499477

9. Donald W. Radford, 3.13 Application of High Temperature Polymer Matrix Composites to Engine Intake Valves, Comprehensive Composite Materials II, Elsevier, 2018, Pages 312-349, ISBN 9780081005347, https://doi.org/10.1016/B978-0-12-803581-8.10339-X.

10. Wong A. A non-adiabatic thermoelastic theory for composite laminates. Journal of Physics and Chemistry of Solids. 31 December 1991; 52: 483–494. Available at: DOI:10.1016/0022-3697(91)90180-8

11. Hooke R., Jeeves TA. 'Direct Search''' Solution of Numerical and Statistical Problems'. J. ACM. New York, NY, USA: Association for Computing Machinery; April 1961; 8(2): 212–229. Available at: DOI:10.1145/321062.321069

REFERENCES

12. Kourehli S., Amiri GG., Ghafory-Ashtiany M., Bagheri A. Structural damage detection based on incomplete modal data using pattern search algorithm. Journal of Vibration and Control. 24 April 2013; 19(6): 821–833. Available at: DOI:10.1177/1077546312438428

13. Swann WH. Direct search methods. Numerical methods for unconstrained optimization. Academic Press New York; 1972; : 13–28.

14. Al-Sumait JS., Al-Othman AK., Sykulski JK. Application of pattern search method to power system valve-point economic load dispatch. International Journal of Electrical Power & Energy Systems. Elsevier; 2007; 29(10): 720–730.

15. Biondi T., Ciccazzo A., Cutello V., D'Antona S., Nicosia G., Spinella S. Multi-Objective Evolutionary Algorithms and Pattern Search Methods for Circuit Design Problems. J. Univers. Comput. Sci. 2006; 12(4): 432–449.

16. Lewis RM., Torczon V., Trosset MW. Direct search methods: then and now. Journal of computational and Applied Mathematics. Elsevier; 2000; 124(1–2): 191–207.

17. Kim W-T., Choi M-Y., Park J-H. Analysis of thermal stress in fatigue fracture specimen using lock-in thermography. Proceedings of the 2006 International Conference on Quantitative InfraRed Thermography. QIRT Council; 2006. Available at: DOI:10.21611/qirt.2006.099

18. Fruehmann RK., Crump DA., Dulieu-Barton JM. Characterization of an infrared detector for high frame rate thermography. Measurement Science and Technology. 1 October 2013; 24(10): 105403. Available at: DOI:10.1088/0957-0233/24/10/105403

19. Daynes S., Potter KD., Weaver PM. Bistable prestressed buckled laminates. Composites Science and Technology. December 2008; 68(15–16): 3431–3437. Available at: DOI:10.1016/j.compscitech.2008.09.036

20. Ruiz-Iglesias R., Ólafsson G., Thomsen OT., Dulieu-Barton JM. Identification of Subsurface Damage in Multidirectional Composite Laminates Using Full-Field Imaging. SEM 2022: Thermomechanics & Infrared Imaging, Inverse Problem Methodologies and Mechanics of Additive & Advanced Manufactured Materials, Volume 6. 2022. pp. 39–42. Available at: DOI:10.1007/978-3-031-17475-9_6

21. Dong C. Development of a Model for Predicting the Transverse Coefficients of Thermal Expansion of Unidirectional Carbon Fibre Reinforced Composites. Applied Composite Materials. 25 May 2008; 15(3): 171–182. Available at: DOI:10.1007/s10443-008-9065-3

EXPERIMENTAL SETUP / Pictures

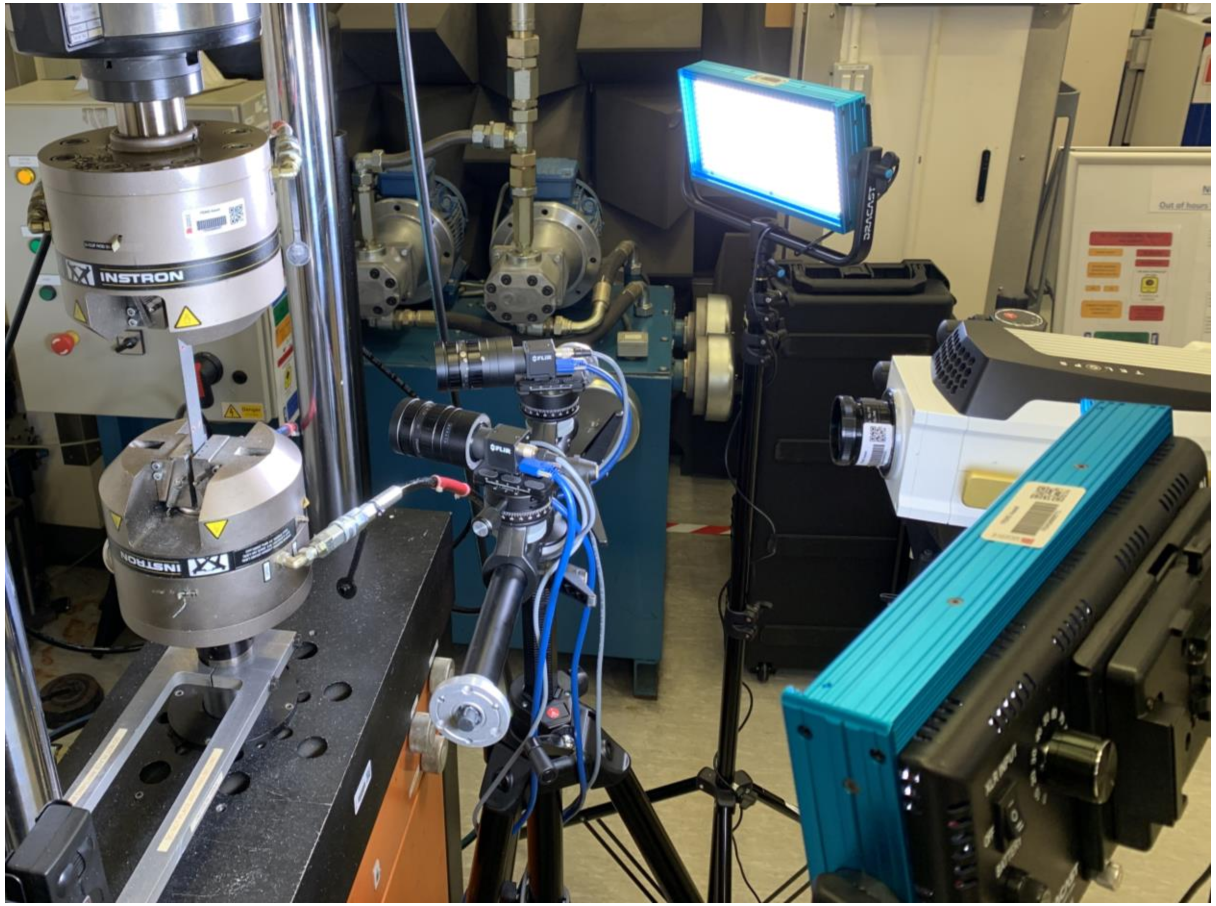

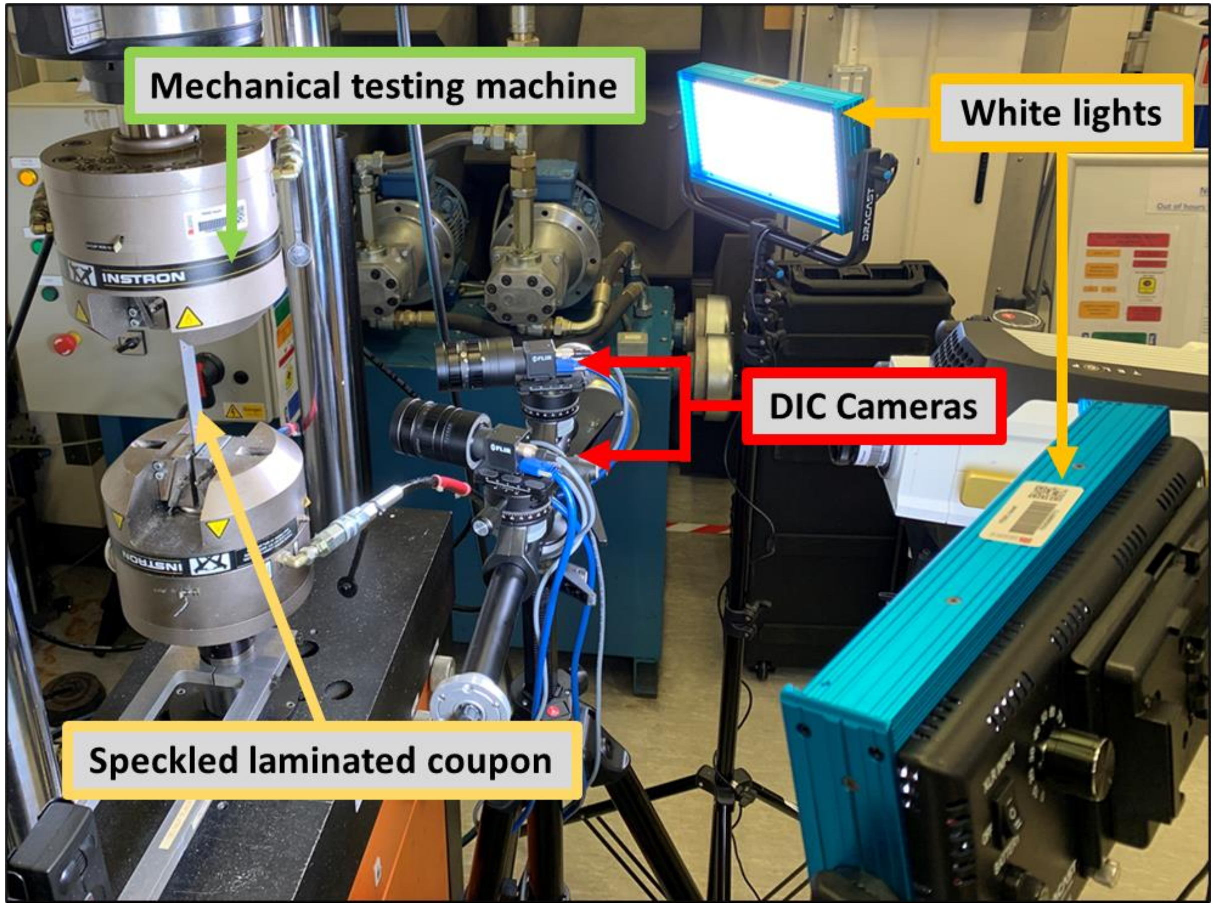

TSA and DIC Data Processing

TSA parameters.

Technique used	Thermal Image Acquisition
Infrared fast camera	Telops Fast M3K
Lens	50 mm
Camera resolution	≈ 20 mK
Pixel to mm conversion	1 px = 0.31 mm
Frames	5250
Frame Rate	383 Hz

DIC parameters and evaluation for testing the unnotched specimens.

Technique used	3D / Stereo Digital Image Correlation	
	Camera 1 (Blackfly-12.3 MPx)	Camera 2 (Blackfly-12.3 MPx)
Sensor, digitalization	Sony IMX226 (CMOS) , 4096 x 3000	
Stereo angle	19.53°	
Frame rate	10 Hz	
Camera noise (% of range)	0.454%	0.443%
Lens and imaging distance	25 mm	25 mm
Total number of images	316	316
DIC software package	MatchID	
Pixel to mm conversion	1 px = 0.0876mm	
ROI (mm)	112.8 x 24.49	
Coordinate transformation	Best-plane-Fit	
Subset, step	13, 10	
Interpolation, shape function, correlation	Bicubic, Quadratic, ZNSSD	
Pre-smoothing	Gaussian Smoothing	
Displacement resolution	$2.176 \cdot 10^{-3}$ mm	
Strain conversion	Log. Euler–Almansi	
Smoothing technique	Local polynomial - affine least-squares fit	
Strain window (pixels)	15 data points	
VSG	153 pixels	
Strain resolution	0.00790%	

HOW IS HEAT TRANSFER OCURRING?

TSA is based on the thermoelastic effect, which describes the coupling between mechanical deformation and thermal energy in an elastic solid and was established by Lord Kelvin (W. Thomson) [4] in 1855

Change in T is proportional to the change of the sum in the principal stresses under adiabatic conditions, and is loaded within the elastic region of the material

$$\dot{T} = \underline{\frac{T_0}{\rho C_\varepsilon}\frac{\partial \sigma_{ij}}{\partial T}\dot{\varepsilon}_{ij}} - \underline{\frac{\dot{Q}}{\rho C_\varepsilon}} \text{ for } i,j = 1,2,3$$

$$\dot{Q} = k\nabla^2 T$$

If $\dot{Q}$ (rate of internal heat generation) = 0 $\longrightarrow$ Adiabatic

To minimise the effect of $\dot{Q}$ (internal heat generation) an **increase in the <u>loading frequency</u>** is required $\longrightarrow$ Increase in $\dot{\varepsilon}_{ij}$

$\longrightarrow$ The $\dot{Q}$ term can be neglected

The thermal diffusion length decrease, and "*pseudo*" adiabatic conditions are achieved

[4] W. Thomson (Lord Kelvin): On dynamical theory of heat, Trans. R. Soc. Edinburgh 20, 261–283 (1853)

IM7/8552 COUPONS MANUFACTURING

- Manufactured in an **autoclave following the manufacturer recommended curing cycles.**
- All panels were made either with peel ply or caul plate: for the peel ply each side of the panels has either a ‘smooth’ surface, which was in contact with the aluminum mold, or a rough surface containing the characteristic peel ply imprint.

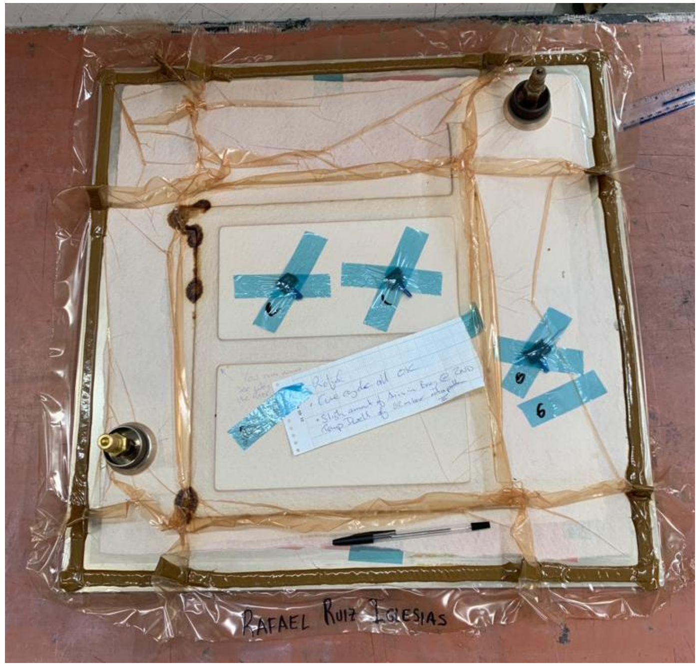

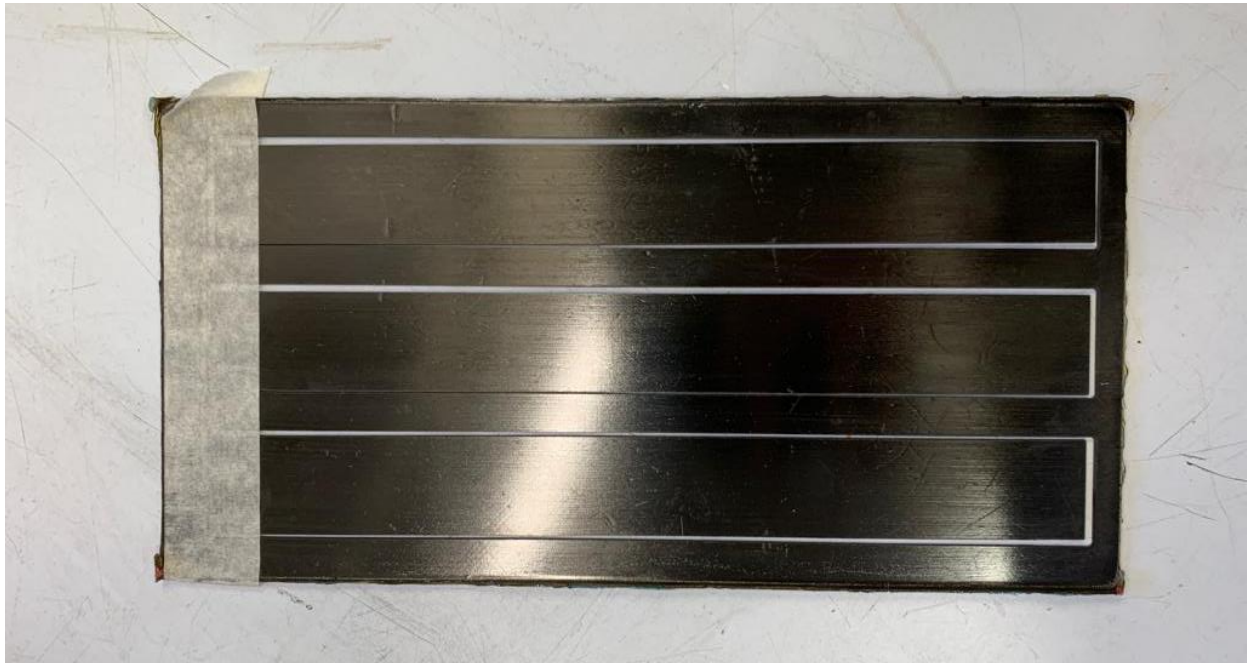

THERMAL CAMERAS / Comparison

Model	Telops FAST IR MK2	FLIR AC655	FLIR Lepton 3.5
Type	Photon Detector	Micro-bolometer	PCB mounted micro-bolometer
Sensor size	256 x 320 pixels	480 x 640 pixels	120 x 160 pixels
Sensitivity	25 mk	50 mK	50 mK
Size	321 × 199 × 176 mm	216 × 73 × 75 mm	10 × 12 × 7 mm
Cost	~ 100k GBP	~10k GBP	~300 GBP

THERMAL CAMERAS / Comparison

Photondetectors datasheet [1]

Characteristics	Photon Detector	
IR Camera	FLIR SC5500	Telops FAST M2k
Detector material	InSb	
Spectral range	2.5 - 5.1 µm	1.5 - 5.4 µm
Pixel dimension	30 µm	25 µm
Cost	~£100,000	
Maximum frame rate at full window	383 Hz	1910 Hz
Frame rate selection	Any value up to 383 Hz	Any value up to 1910 Hz
Reading array	All pixel detectors at the same time	
Integration time	10 - 20,000 µs	0.27 µs to 513 µs
Response time	10 - 20,000 µs	0.27 µs to 513 µs
Sensitivity (NETD)	<20 mK	<25 mK
Resolution	320 x 256 pixels	
Cooling	Yes	
Analogue input	Yes	
Weight	3.8 kg	< 6 kg
Size	310 x 141 x 159 mm	321 x 199 x 176 mm

Microbolometers datasheet [1]

Characteristics	Standard microbolometer	Thermal core microbolometer
IR Camera	FLIR A655sc	FLIR Lepton 3.5 radiometric
Detector material	VOx	VOx
Spectral range	7.5 - 14 µm	8 - 14 µm
Pixel dimension	17 µm	12 µm
Cost	~£10,000	~£500
Maximum frame rate at full window	50 Hz	Limited at 8.7751 Hz
Frame rate selection	50 Hz, 25 Hz, 12.5 Hz, 6.25 Hz, 3.13 Hz	8.7751 Hz
Reading array	Each row of pixels at a time	
Thermal time constant	8 ms - fixed	12 ms
Response time	24 ms (3 x thermal time constant)	36 ms (3 x thermal time constant)
Sensitivity (NETD)	< 30 mK	< 50 mK
Resolution	640 x 480 pixels	160 x 120 pixels
Cooling	No	
Analogue input	No	
Weight	0.9 kg	0.9 g
Size	216 x 73 x 75 mm	10.50 x 12.70 x 7.14 mm

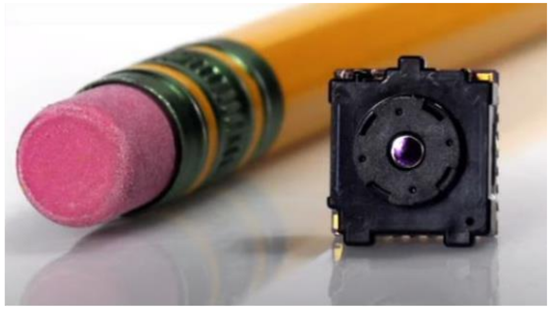

FLIR Lepton 3.5 radiometric

[1] Irene Jiménez-Fortunato. Development and integration of full-field imaging techniques for assessment of composite structures. 2021.

Micromechanical Models considerations

Schapery model

$$\alpha_{22} = (\alpha_{fT} + \alpha_{fL} \nu_f) V_f + \alpha_m (1 + \nu_m)(1 - V_f) - \alpha_{11} [\nu_f V_f + \nu_m (1 - V_f)]$$

based on the simple planar model of alternating fibre and matrix strips.

Modified strip model

$$\alpha_{22} = \frac{(\alpha_{fT} + \alpha_{fL} \nu_f) V_f + \alpha_{fT} \nu_{fTT} \sqrt{V_f} + \alpha_m [1 - V_f + \nu_m (2 - V_f - \sqrt{V_f})] - \alpha_{11} [\nu_f V_f + \nu_m (1 - V_f)]}{1 + \nu_{fTT} \sqrt{V_f} + \nu_m (1 - \sqrt{V_f})}$$

developed based on Schapery model by introducing the constraint effects from thermal expansion and Poisson's ratio mismatch of fibre and matrix.

Chamis model

$$\alpha_{22} = \alpha_{fT} \sqrt{V_f} + \alpha_m (1 - \sqrt{V_f}) \left(1 + V_f \nu_m \frac{E_{fT}}{E_{11}}\right)$$

developed based on a simple force-balance.

Hashin's concentric cylinder model

$$\alpha_{22} = \widehat{\alpha}_{22} + \left(\overline{S}_{12} - \widehat{S}_{12}\right) [(\alpha_{fL} - \alpha_m) P_{11} + 2(\alpha_{fT} - \alpha_m) P_{12}]$$
$$+ \left(\overline{S}_{22} - \widehat{S}_{22}\right) [(\alpha_{fL} - \alpha_m) P_{12} + (\alpha_{fT} - \alpha_m)(P_{22} + P_{23})]$$
$$+ \left(\overline{S}_{23} - \widehat{S}_{23}\right) [(\alpha_{fL} - \alpha_m) P_{12} + (\alpha_{fT} - \alpha_m)(P_{22} + P_{23})]$$

developed from a cylinder assemblage model.

where $\mathbf{S}$ is the compliance matrix. Terms with an overbar and hat refer to effective and average composite properties.

$$P_{11} = (A_{22}^2 - A_{23}^2)/\det \mathbf{A}$$
$$P_{12} = (A_{12} A_{23} - A_{22} A_{12})/\det \mathbf{A}$$
$$P_{22} = (A_{11} A_{22} - A_{12}^2)/\det \mathbf{A}$$
$$P_{23} = (A_{12}^2 - A_{11} A_{23})/\det \mathbf{A}$$
$$\mathbf{A} = \mathbf{S}^{(\mathrm{f})} - \mathbf{S}^{(\mathrm{m})}$$
$$\det \mathbf{A} = A_{11}(A_{22}^2 - A_{23}^2) + 2A_{12}(A_{12} A_{23} - A_{22} A_{12})$$

ALL IM7/8552 Properties

Layups	$[0, 0, 0, 45, -45, 0]_s$, $[0, 45, -45, 0, 0, 0]_s$
Loading frequencies (Hz)	0.5, 1.1, 2.1, 3.1, 4.1, 5.1, 6.1,7.1,8.1,9.1,10.1,12.1, 15.1, 17.1, 20.1, 22.1, 25.1, 27.1, 30.1
Ply thickness (mm)	0.125
Resin layer thickness (μm)	5, 8
Experimental sampling frequency (Hz)	383.0

Property	IM7/8552
Young's modulus E_1 (GPa)	159.5*
Young's modulus E_2 (GPa)	10.1*
Poisson's ratio ν_{12}	0.325*
Shear modulus G_{12} (GPa)	5.14*
Thermal expansion coeff. α_1 (10^{-6} K^{-1})	**-0.102***
Thermal expansion coeff. α_2 (10^{-6} K^{-1})	**23.138***
Thermal conductivity k_1 (W m K^{-1})	5
Thermal conductivity k_2 (W m K^{-1})	0.82
Density ρ (Kg dm^{-3})	1.5692*
Specific heat C_ε (J Kg^{-1} K^{-1})	884.53

Property	Epoxy resin
Young's modulus E (GPa)	3.8
Poisson's ratio ν	0.35
Shear modulus G_{12} (GPa)	2.71
Thermal expansion coeff. αr (10^{-6} K^{-1})	53.5
Thermal conductivity k (W m K^{-1})	0.2
Density ρ (Kg dm^{-3})	1.153
Specific heat C_ε (J Kg^{-1} K^{-1})	1110

Measuring the $K_{t.thickness}$ (The Flash Method)

Main literature reference: 0.84 W/m*K [5]

[5] M.T. Saad, S.G. Miller, T. Marunda, Thermal characterization of IM7/8552-1 carbon-epoxy composites, ASME 2014 Int. Mech. Eng. Congr. Expos. (2014) 1–8.

Table 1. Thermal Properties of IM7/8552-1 Composite

Temperature (°C)	Thermal Diffusivity (cm^2/s)	Specific Heat (J/g*K)	Thermal Conductivity (W/m*K)
25	0.0068	0.85741	0.84126
50	0.0067	0.91981	0.88184
75	0.0065	0.98683	0.92572
100	0.0064	1.05835	0.97286
125	0.0063	1.13099	1.02034
150	0.0062	1.20378	1.06764
175	0.0061	1.28975	1.12186

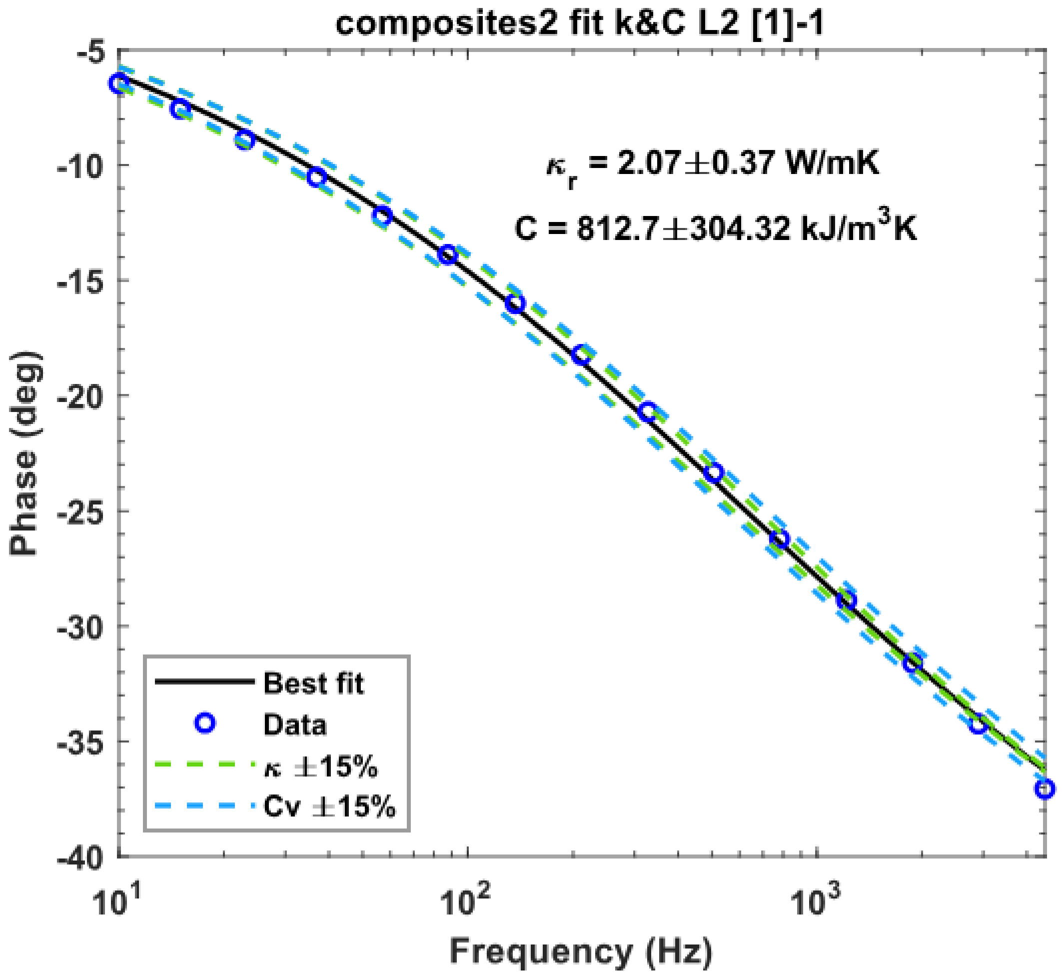

The flash method

- The power source can be a laser or a flash lamp.
- The energy will then be absorbed by the specimen and emitted again on the top of the sample.
- This radiation results in a temperature rise on the surface of the sample.
- This temperature rise is recorded from an infrared (IR) detector.

The Flash Method

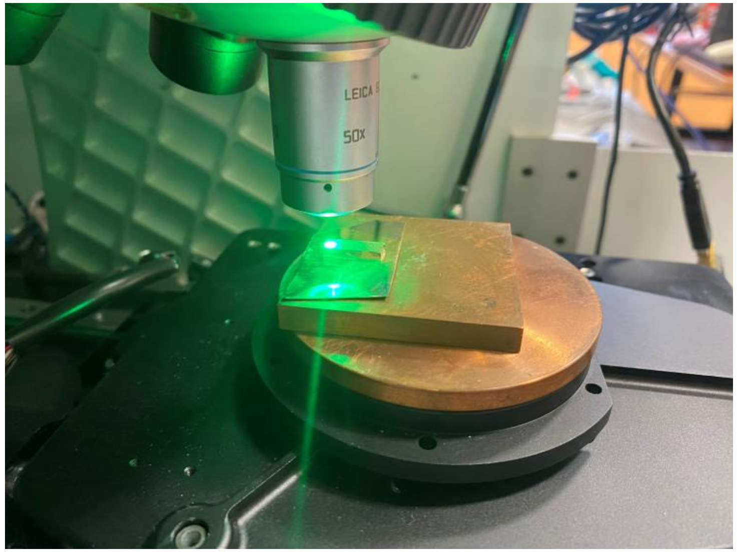

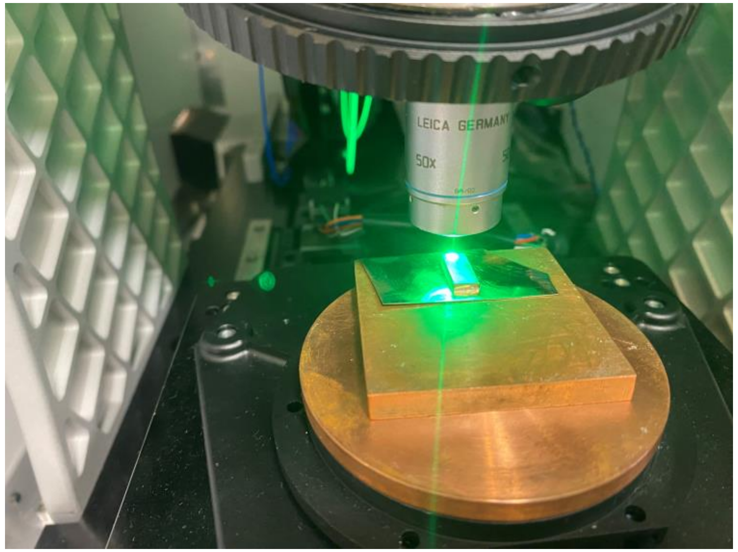

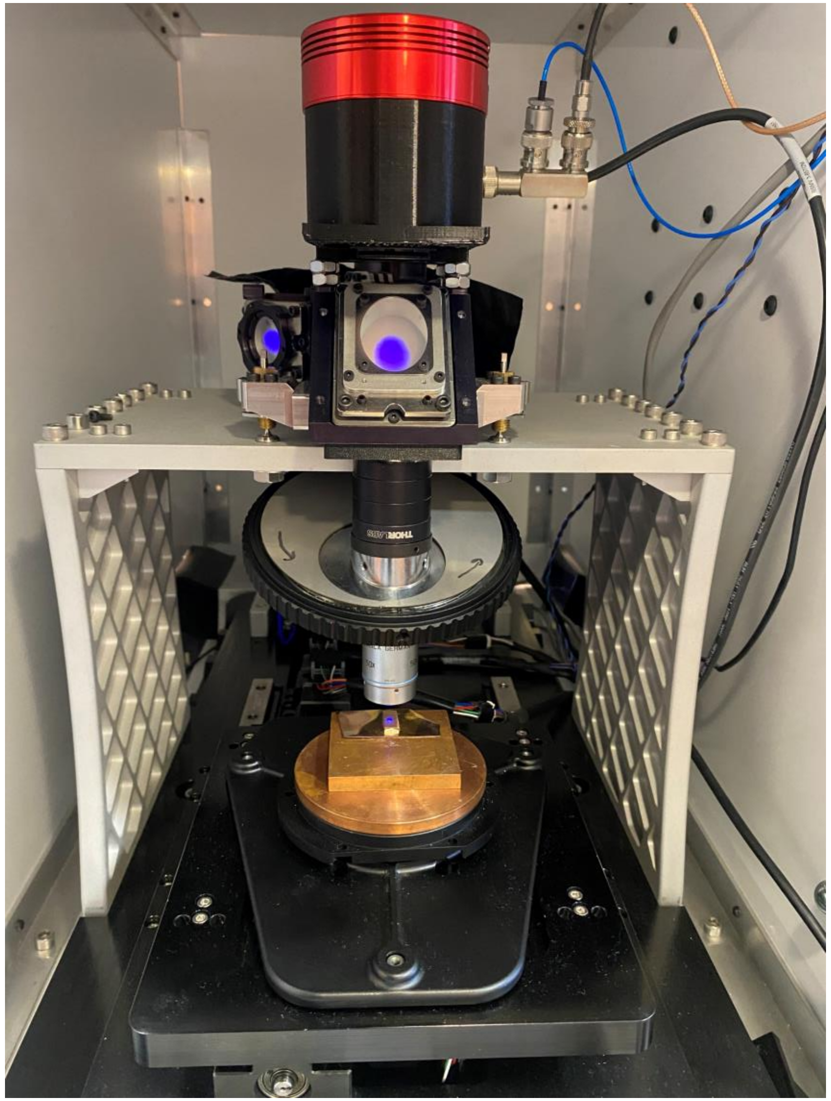

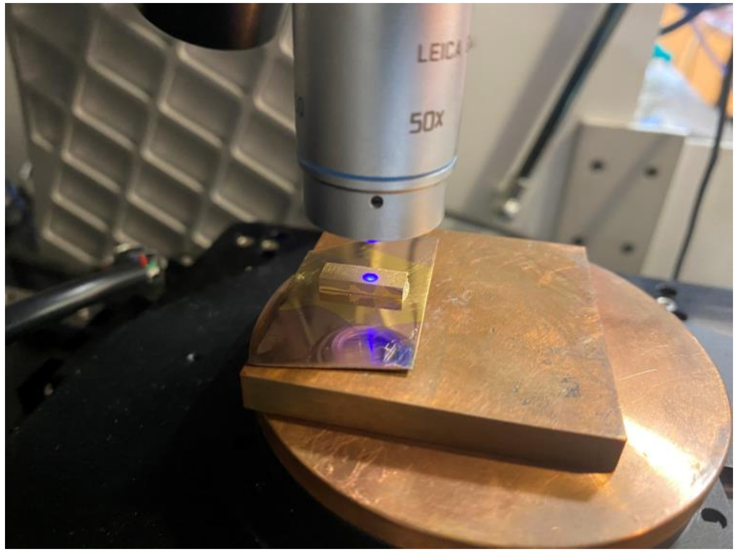

Lock-in filtering approach

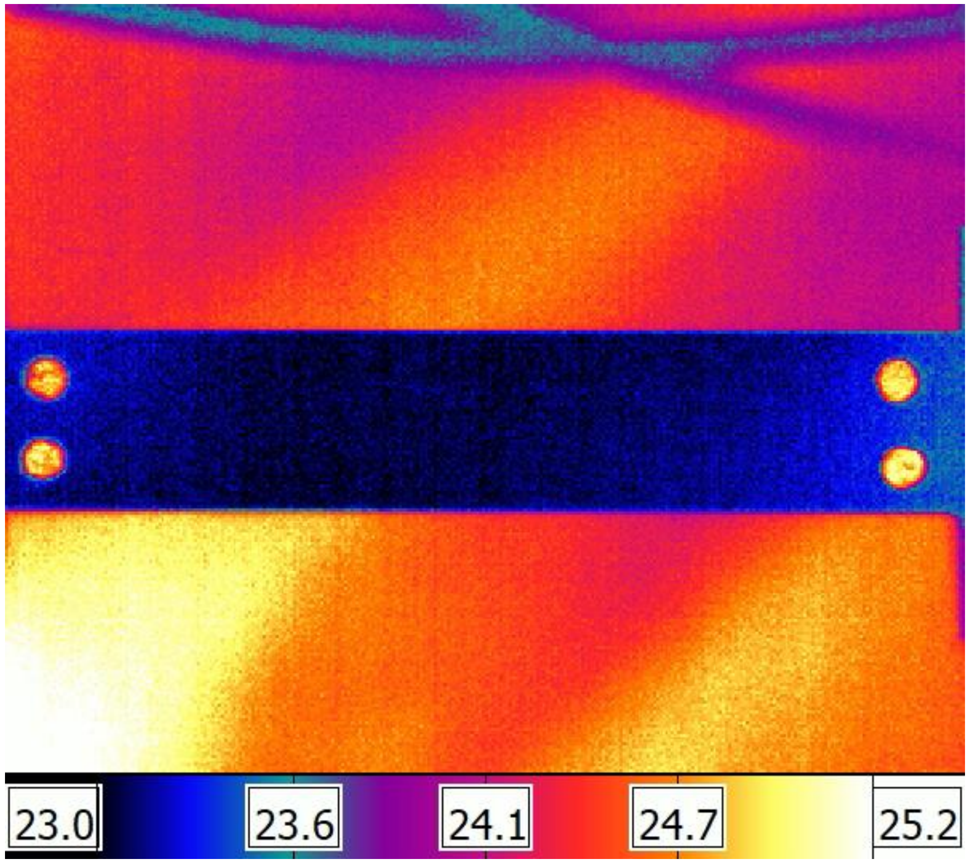

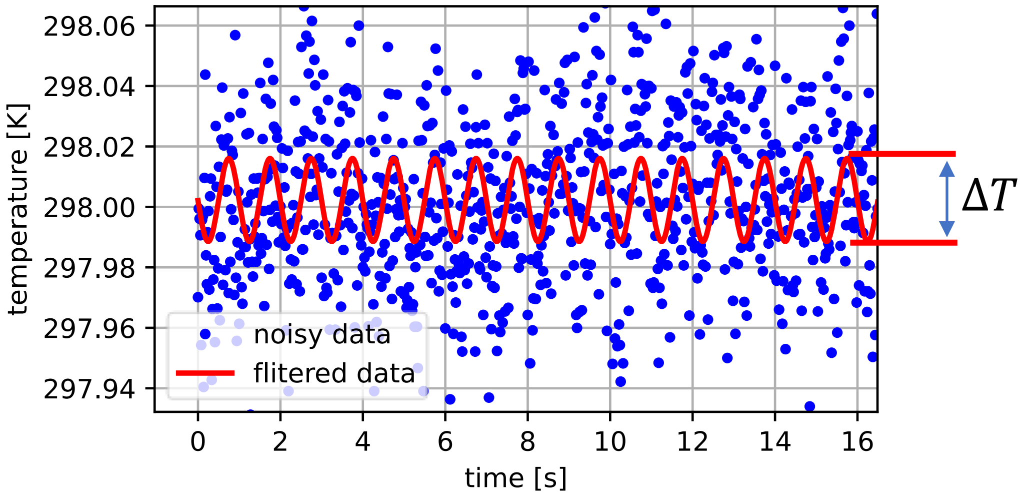

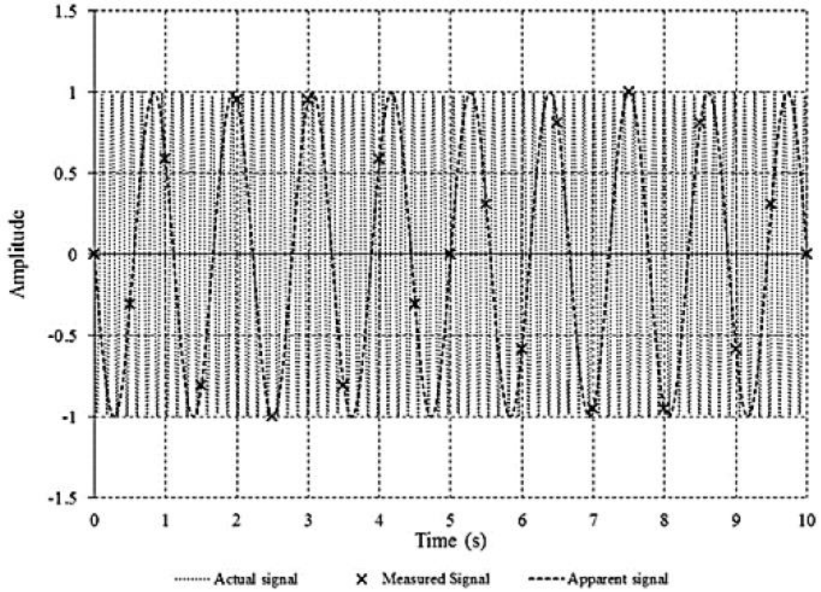

$[0,45,-45,0,0,0]_S$

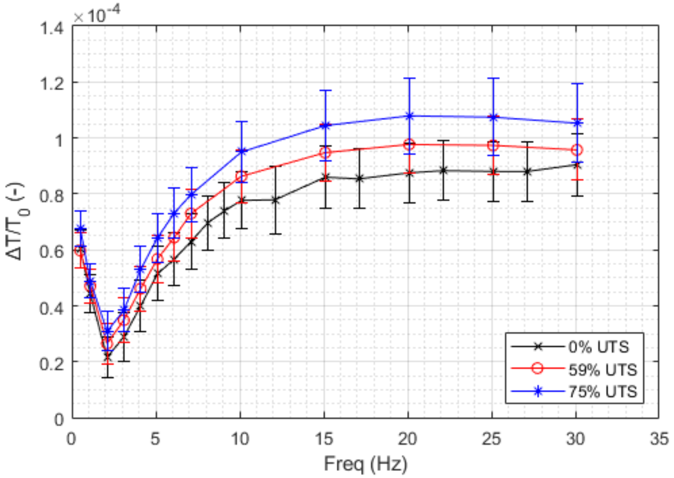
×10⁻⁴
ΔT/T₀ (-)
Freq (Hz)
0% UTS
59% UTS
75% UTS

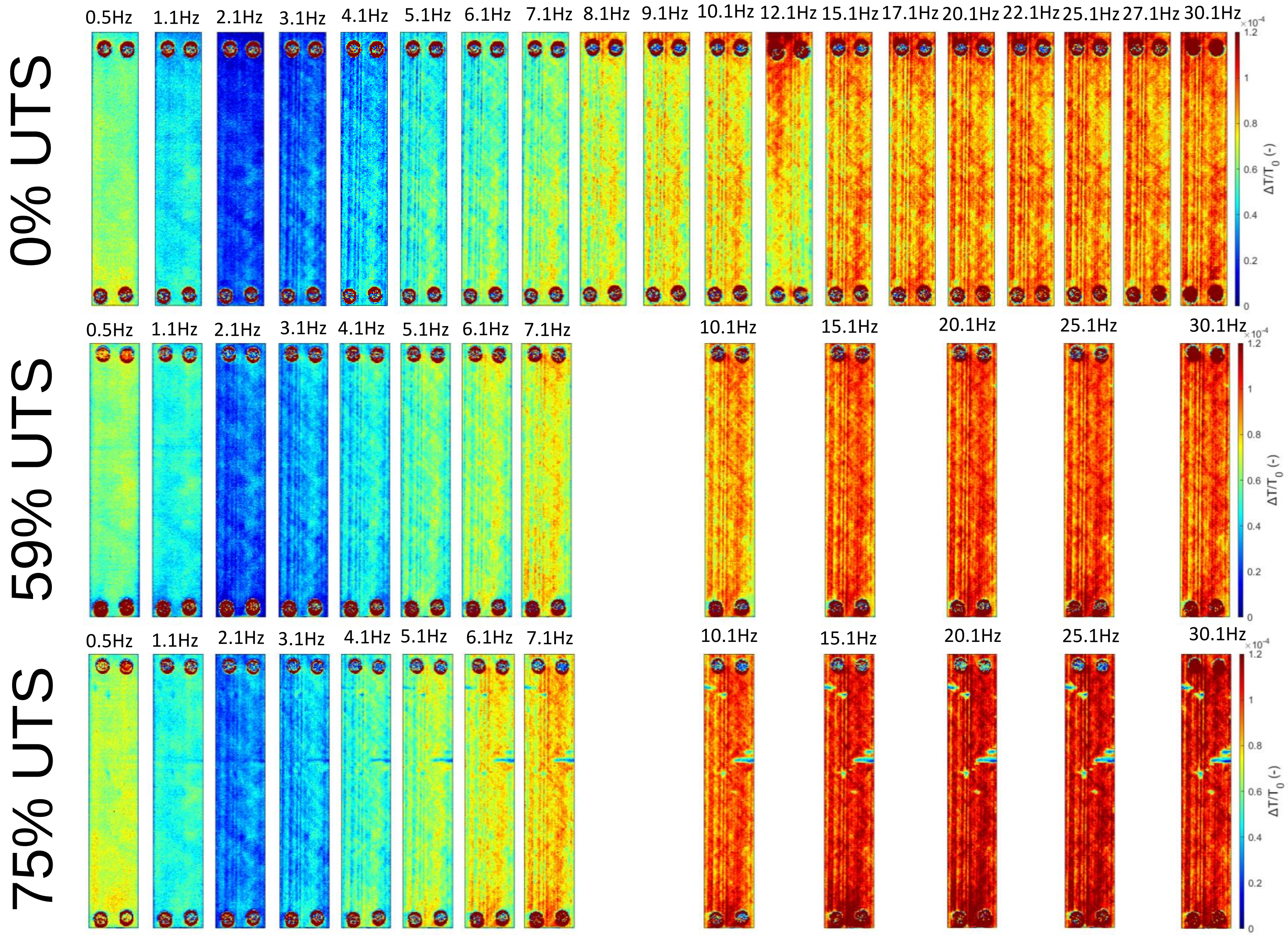
0% UTS
0.5Hz 1.1Hz 2.1Hz 3.1Hz 4.1Hz 5.1Hz 6.1Hz 7.1Hz 8.1Hz 9.1Hz 10.1Hz 12.1Hz 15.1Hz 17.1Hz 20.1Hz 22.1Hz 25.1Hz 27.1Hz 30.1Hz
59% UTS
0.5Hz 1.1Hz 2.1Hz 3.1Hz 4.1Hz 5.1Hz 6.1Hz 7.1Hz 10.1Hz 15.1Hz 20.1Hz 25.1Hz 30.1Hz
75% UTS
0.5Hz 1.1Hz 2.1Hz 3.1Hz 4.1Hz 5.1Hz 6.1Hz 7.1Hz 10.1Hz 15.1Hz 20.1Hz 25.1Hz 30.1Hz
ΔT/T₀ (-)

$[0,0,0,45,-45,0]_s$

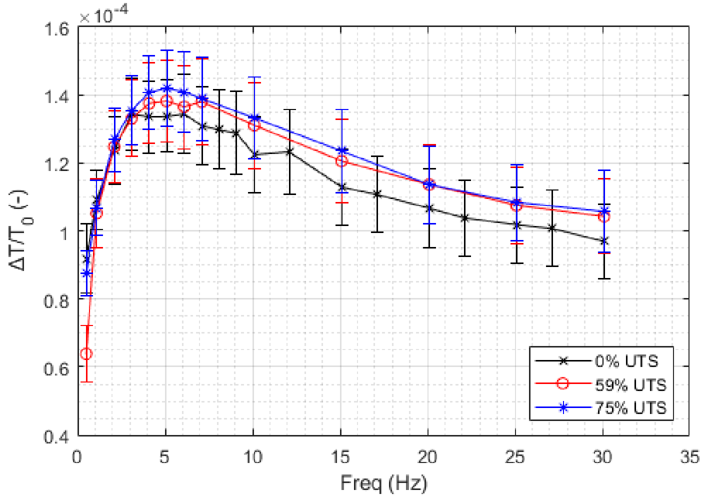

×10^-4
1.6
1.4
1.2
1
0.8
0.6
0.4
ΔT/T0 (-)
0
5
10
15
20
25
30
35
Freq (Hz)
0% UTS
59% UTS
75% UTS

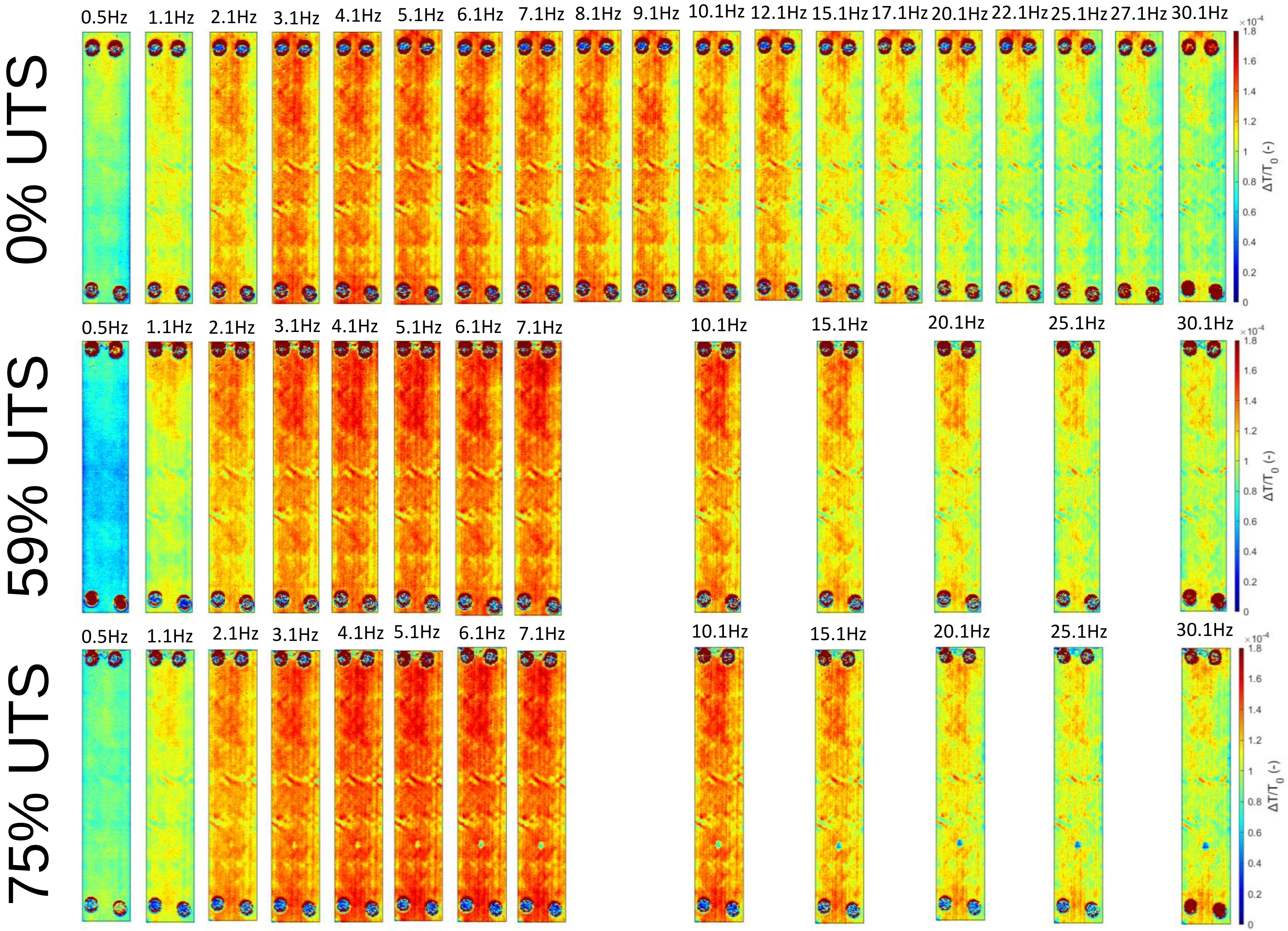

0% UTS
59% UTS
75% UTS
0.5Hz
1.1Hz
2.1Hz
3.1Hz
4.1Hz
5.1Hz
6.1Hz
7.1Hz
8.1Hz
9.1Hz
10.1Hz
12.1Hz
15.1Hz
17.1Hz
20.1Hz
22.1Hz
25.1Hz
27.1Hz
30.1Hz
ΔT/T0 (-)

The resin influence on Strip specimens TSA Results

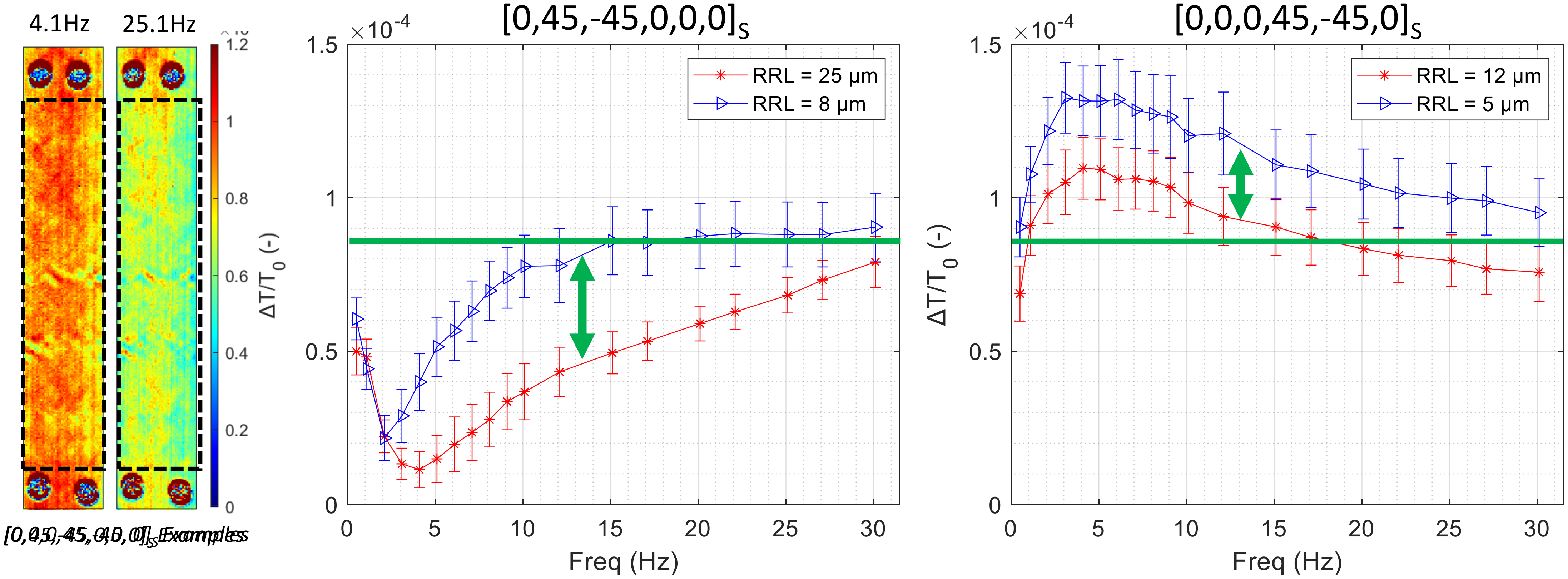

The trend of ***$\Delta T/T_0$* is different for the two configurations** with loading frequency.

Both layups **"converge" to a similar level** at high frequencies.

The **RRL** has an influence on *ΔT* and **changes the response** in this frequency domain (0.5 – 30.1 Hz).

Wong's model considerations

T_0 ~ Mean temperature
ρ ~ Density
C_p ~ Specific heat capacity
α_1 and α_2 ~ Thermal expansion coefficients in 1,2
$\Delta\sigma_1$ and $\Delta\sigma_2$ ~ Stress variation in 1,2
$[Q]_{1,2}$ ~ Stiffness matrix
$[T]$ ~ Transformation matrix
$[\Delta\varepsilon_{xy}]$ ~ Strain variation in x,y

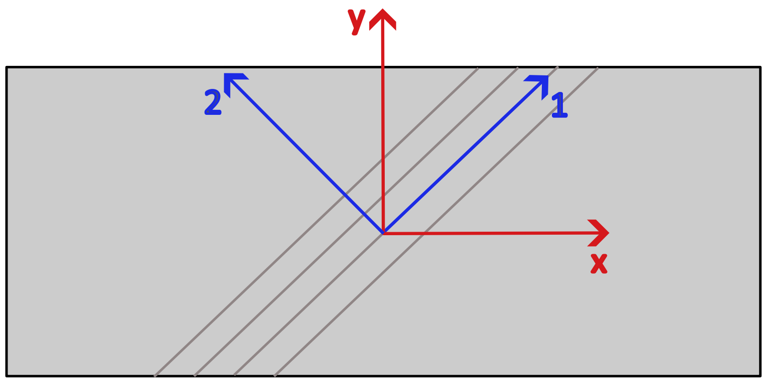

1,2: Ply coordinate system

x,y: Laminate coordinate system

$$\Delta T = \frac{-T_0}{\rho C_p}(\alpha_1\Delta\sigma_1+\alpha_2\Delta\sigma_2) = \frac{-T_0}{\rho C_p}\left([\alpha]^T_{1,2}[Q]_{1,2}[T][\Delta\varepsilon]_{xy}\right)$$

Simplified for orthotropic composite lamina (as $\alpha_6 = 0$)

There are **models** that aim to replicate the thermoelastic behaviour of composites

A.K. Wong [10]: A non-adiabatic thermoelastic theory for composite laminates (numerical model):

- 1-D model
- Conduction process is described by numerically solving the 1-D diffusion equation

Assuming that heat transfer during thermoelastic cycling is dominated by diffusion in the through- thickness direction

- Considers layers orientation, loading frequency, the resin surface layer thickness and the cyclic stress regime
- This model was validated for CFRP [0,45,-45] at a frequency range of 5-30 Hz